Genomic rearrangements rewire chromatin contacts and drive adaptive gene expression divergence in mammals

Jui Bhattacharya, Mohan Lal, Kuljeet Singh Sandhu*

Department of Biological Sciences
Indian Institute of Science Education and Research (IISER)- Mohali
Knowledge City, Sector 81, SAS Nagar 140306, Punjab, India.

*sandhuks@iisermohali.ac.in

Keywords: Genomic rearrangements, mammalian evolution, clade-specific traits

Running title: Adaptive genome rewiring in mammals

Abstract

Genomic rearrangements (GRs) are pervasive in mammalian evolution, yet their contribution to adaptive trait divergence remains poorly defined. By examining 71 mammalian genomes across eight major clades, we uncovered 206 clade-specific disruptions of ancestral synteny. These rearrangements consistently localize near genes underpinning clade-specific physiological, metabolic and behavioural traits and coincided with the accelerated expression rates in the affected lineage. The disruption of otherwise syntenic chromatin contacts and the fusion of domains with contrasting epigenetic states implied that the alteration in regulatory adjacency may underlie the expression divergence. Primate-specific rearrangements exhibited signatures of selective constraint, including fixation across species, reduced recombination, elevated linkage disequilibrium, and enhanced co-expression of genes flanking rearranged loci, indicating that these genomic architectures are selectively maintained. Our observations imply that the clade-specific genomic rearrangements repeatedly reconfigured the mammalian regulatory landscape and likely served as an evolutionary substrate for lineage-specific adaptation.

67 **Introduction**

68 Genomes have gone through several rounds of structural rearrangements during the
69 course of evolution. These rearrangements reshape the genome order and,
70 therefore, may change the regulatory context of the genes. Such alterations may
71 lead to expression divergence, of genes popularly known as chromosomal position
72 effect(Wallrath and Elgin 1995; Elgin and Reuter 2013). Ectopic position effects can
73 lead to diseases in human and mice(Milot et al. 1996; Kleinjan and Van Heyningen
74 1998). For example, translocation breakpoint between PAX6 and its downstream
75 regulatory elements associates with Aniridia in human(Fantes et al. 1995). A
76 genomic rearrangement at 100kb upstream to Steel(Sl) locus downregulates Mgf
77 gene and causes sterility in female mice(Bedell et al. 1995) . Similarly breakpoints
78 near SOX9, TWIST, and RIEG genes have association with campomelic dysplasia,
79 Saethre-Chotzen, and Rieger syndromes respectively in human(Wirth et al. 1996;
80 Krebs 1997; Flomen et al. 1998). Yet the evolutionary implications of chromosomal
81 position effects remain largely under appreciated. De et al had shown that
82 expression divergence associated with the position effects may contribute to
83 phenotypic differences between human and chimpanzee(De et al. 2009). Bagadia et
84 al showed that the genomic rearrangements may explain the evolutionary
85 divergence of some brain related traits in rodents(Bagadia et al. 2019). Recently,
86 Real et al(Real et al. 2020) identified genomic rearrangements that altered the
87 regulatory context of gonadal gene expression governing intersexuality in moles.
88 These studies were limited by the number of species analysed and by the context of
89 genomic rearrangements. With the availability of large number of mammalian
90 genomes, it is now possible to examine the phenotypic associations of genomic
91 rearrangements in mammals. Through analysis of 71 mammalian genomes
92 representing 8 clades, we identified 206 clade-specific long-range genomic
93 rearrangements marking evolutionary loss of synteny. We found that the clade-
94 specific breakpoints flanked by the genes associated with specific phenotypes of
95 respective clades. The clade-specific breakpoints frequently disrupted the conserved
96 enhancer-promoter communications, which coincided with the diverged expression
97 rates of the flanking genes. Our observations implied the wide-spread adaptive
98 significance of genomic rearrangements in mammals.
99

100 **Results**

101 By applying the strategy outlined in the Methods section, we first identified all
102 pairwise instances of long range (>10 Mb and *trans*) genomic disruptions of synteny
103 across 71 mammals(Figure 1). The phenogram and the Disparity-Through-Time
104 (DTT) plots of mean GR frequencies suggested divergence of evolutionary rate of
105 GRs in artiodactyls, cetaceans, and rodents when compared to the rates expected
106 under Brownian Motion (BM) model (Figure 2a-b). Following the strategy given the
107 methods section, we further identified 206 clade-specific evolutionary breakpoint
108 regions (EBRs) engaged in loss-of-synteny (LoS) events (Figure 2c). Rodents and
109 artiodactyls exhibited the most numbers of clade-specific loss-of-synteny (cs-LoS)
110 events (94 and 38 respectively), which were consistent with the earlier reports (Luo
111 et al. 2012; Kim et al. 2017). More than 90% of gene-pairs flanking clade-specific
112 breakpoints were syntenic in the eutherian ancestor(Kim et al. 2017), validating our
113 inference of ancestrally syntenic configuration of the identified cases (Figure S1)
114

115 To assess if the cs-LoS EBRs position preferably near certain functional loci, we
116 obtained the genes within and the flanking 10 genes on the either sides of cs-LoS
117 EBRs. Gene ontology analysis yielded enrichment of clade-specific functional terms.
118 Primates exhibited enrichment of glucocorticoid secretion (CRHR1, TAC1, CRY1
119 etc.), lipid transport, synaptic transmission and behaviour related terms (SHANK2,
120 RELN, FOXP1, GIT1, KLHL1, NRG1, MAPT etc.) (Figure 3). These functions have
121 associations with primate-specific trait divergence(Bozek et al. 2015; Muntané et al.
122 2015; Dunn-Fletcher et al. 2018; Spanaki et al. 2024). The genes flanking
123 artiodactyl-specific LoS break-points were enriched with flavonoid and lipid
124 metabolism related terms, including genes like UDP-glucuronosyltransferase 1A
125 (UGT1A) and Fatty Acid Binding Protein 4 (FABP4) (Figure 3). These terms
126 associate with vegetarian diet and musculoskeletal health respectively, which
127 coincide with herbivory and relatively large body mass of artiodactyls(Jiang et al.
128 2014; Kawai et al. 2021). Carnivore-specific LoS exhibited enrichment of extra-
129 cellular matrix proteins, particularly matrix metalloproteases (MMPs) (Figure 3). It is
130 established that carnivores, unlike other mammals, have endotheliochorial
131 placenta(Wooding and Burton 2008). Differential expression of MMPs is the hallmark
132 of invasive placentation in carnivores(Diessler et al. 2017). We further hypothesize
133 that enrichment and expression divergence of MMPs in carnivores may also relate to

134 effective wound healing in carnivores being susceptible to frequent wounds due to
135 predation and the territory defence. Rodents exhibited enrichment of renal filtration
136 related terms, aligning to their higher glomerular filtration rate, which is an adaptation
137 to physiological requirements in diverse habitats and dietary habits of
138 rodents(Dickinson et al. 2007; Benjamin et al. 2015; Bittner et al. 2021). The term
139 includes the genes Anillin, Glucocorticoid Induced 1 (GLCCI1), Thrombospondin
140 type-1 domain-containing 7A (THSD7A), Apolipoprotein L1 (APOL1) etc., which have
141 strong associations with renal filtration and implicate in kidney diseases(Nishibori et
142 al. 2011; Gbadegesin et al. 2014; Tomas et al. 2014; Pays 2021). Top enriched
143 genes in Chiroptera-specific LoS break-points exhibited immunity related functions,
144 adhering to pronounced immune tolerance in bats(Sulak et al. 2016; Jebb et al.
145 2020). Among others, we also observed genes like CEBPA and TNFRSF1A that are
146 associated with echolocation in bats(Hudson et al. 2014; Wang et al. 2019). The
147 cetacean break-points show weak enrichment of r-RNA processing and sterol related
148 functions, aligning to longevity, body mass and diverged metabolism of
149 cetaceans(Doherty and de Magalhães 2016; Derous et al. 2021) Afrotheria-specific
150 LoS showed moderate enrichment of potassium ion channels, vitamin-K metabolism,
151 and the blood coagulation (Figure 3). Ion transporters are linked to the cell
152 proliferation, cell size and cancer, the traits significantly diverged in afrotheria
153 clade(Savage et al. 2007). Vitamin-K is linked to the osteoblast differentiation, likely
154 associated with the larger body mass of afrotherians like elephant, manatee etc.
155 Blood coagulates faster in elephants(Lewis 1974) and the presence of blood
156 coagulation factors in our set might mark an adaptation against an ancient fatal
157 haemorrhagic disease caused by elephant endotheliotropic herpesvirus(Guntawang
158 et al. 2021). Similarly, perissodactyl-specific breakpoints showed moderate
159 enrichment of eye development and aerobic respiration, which lines up with the large
160 size, 350° visual field, unique motion sensitivity of horse eye(Roth and McGreevy
161 2025), and remarkably high aerobic respiration capacity of equine lungs(Poole and
162 Erickson 2011) (Figure 3).
163
164 In most clades, genes proximal to the cs-LoS breakpoints exhibited the expression
165 divergence from that of the phylogenetically proximal clade controlled through an
166 outgroup, implying the adaptive significance of genomic rearrangements (Figure 4).

167 The chromosomal position-effect may explain the observed expression divergence.
168 To test this, we first analysed the chromosomal coordinates of enhancer-promoter
169 pairs that exhibited evolutionarily conserved synteny. We observed non-random
170 accumulation of clade-specific breakpoints within enhancer-promoter spans, which
171 were syntenic in other clades, suggesting that the expression divergence of genes
172 might have been driven by the loss of proximity to their cognate enhancers (Figure
173 5a-b). Secondly, we assessed the position effect through analysis of chromatin
174 compartments. We observed that the chromatin compartments with contrasting
175 states (A and B) in a species tended to fuse together and subsequently exhibited a
176 coherent state (A or B) in the species exhibiting cs-LoS event (Figure 5c-d). This is
177 marked by a decrease in Kronecker's delta (Methods) of consecutive genomic bins
178 around breakpoints (Figure 5c). This may signify an alteration in gene expression
179 through the mixing of contrasting epigenetic states *via* gained proximity. We
180 illustrated this through an example of primate-specific genomic rearrangement near
181 Neurokinin-1 (TAC1), a glucocorticoid secretion and behaviour related gene. The
182 gene locates in the B-compartment in mouse, which gains proximity to an A-
183 compartment, and subsequently switches from B-to-A compartment in neuronal cells
184 (Figure 5d). Overall the split of enhancer-promoter synteny and gain of proximity
185 between A and B chromatin compartments highlight the mechanistic basis of
186 expression divergence of genes located near cs-LoS breakpoints.
187
188 We further exemplified a primate-specific LoS event near Corticotropin Releasing
189 Hormone Receptor 1 (CRHR1) gene that coordinates the autonomic, endocrine and
190 behavioural response to stress and depression through Hypothalamus-Pituitary-
191 Adrenal (HPA) axis(Jezova et al. 1999) and may also regulate the timing of
192 birth(Smith and Nicholson 2007). Interestingly, CRHR1 shows primate-specific
193 conservation of 29 amino acids of exon-6, and insertions of retroviral LINE elements
194 at the upstream region (Figure S2). The gene also exhibits loss of chromatin
195 contacts and expression divergence in primates (Figure 6a-b). We propose that the
196 sequence and the expression divergence of this locus may link to primates'
197 adaptation to stress from complex social structures(Pusey et al. 1997; Sapolsky
198 2021). Similarly, artiodactyl-specific LoS near UGT1A genes, which metabolizes
199 flavonoids commonly present in vegetarian diet, exhibited disruption of chromatin
200 contacts and expression divergence in artiodactyls (Figure 6c-d). UGT1A genes

have expanded copy numbers in herbivores(Kawai et al. 2021), implying convergence of distinct molecular mechanisms underlying expression evolution of UGT1A genes in artiodactyls.

To assess whether the clade-specific GRs are shaped by selection, we focused on primate-specific LoS events, leveraging the available population genomic data. We found that rearranged loci exhibit elevated linkage disequilibrium and reduced recombination rates around primate-specific fusion points in humans, indicating tight genetic linkage (Figure 7a-b). These rearrangements also displayed fixed genomic adjacencies across primates (Figure 7c). In addition, genes flanking primate-specific fusion points show stronger co-expression compared with genes near corresponding primate-specific LoS breakpoints in a non-primate species (mouse) (Figure 7d). Together, these patterns are consistent with the selective constraints acting on primate-specific GRs and may extend to other clades.

Discussion

Genes are not autonomous transcriptional units within the genomic landscape but rather operate in a highly context-dependent manner influenced by their local and global chromatin environment. Reporter integration in proximity to enhancer strengthens the expression, while that within lamina-associated domains attenuates the transcriptional activity(Akhtar et al. 2013). Distinct linear and spatial positions of a gene also confer variation to its expression noise(Chen and Zhang 2016; Singh et al. 2016). The alterations in genomic context through chromosomal rearrangements can, therefore, influence the epigenetic and transcriptional states of the genes. Although studied in somatic human cells and cancer tissues(Chiang et al. 2017; Xu et al. 2022), the evolutionary dynamics of such position effects remains poorly understood. Our observations through this study highlight that the clade-specific long-range genomic rearrangements associate with the enrichment and expression-divergence of genes with clade-defining traits. Interestingly, these genes have also lost the proximity to their cognate enhancers as reflected from the splitting of enhancer-promoter pairs, likely representing one of the possible causes of the observed divergence of gene expression in the respective clades. The gained proximity of chromatin domains with opposing epigenetic states further strengthens the notion of chromosomal position effect in evolutionary context. We propose that

235 the alteration in regulatory context may have contributed to the expression evolution
236 of genes proximal to clade-specific EBRs. From our observations, it follows that
237 clade-specific GRs may have guided the evolution of clade-specific mammalian
238 phenotypes through gene expression evolution. Primate-specific fixation and tight
239 linkage of rearranged loci further implied the signatures of selective constraints.
240
241 The reported genomic rearrangements and the engaged loci also offer a valuable
242 catalogue for biomedical interpretation. Many of the reported loci also implicate in
243 human diseases and understanding the rewiring of their regulatory contexts could
244 help in genetic prioritization and devising medical strategies to intervene the mis-
245 regulation. Certain mammals are resistant to certain diseases, like elephant is
246 resistant to cancer and bats are immune tolerant to viruses. Our observations may
247 also help studying the regulatory contexts which are instrumental in disease
248 resistance and exploit that knowledge to understand disease susceptibilities in
249 humans.
250

251 Conclusion

252 Altogether, our observations suggest that clade-specific genomic rearrangements
253 are not merely the passive signatures of evolutionary history and speciation but are
254 active agents reshaping mammalian regulatory landscapes. By rewiring enhancer-
255 promoter contacts and shuffling chromatin compartments, these rearrangements
256 generate lineage-specific expression programs that coincide with the emergence of
257 clade-defining phenotypes. The recurrence of such events across distant
258 mammalian clades highlights genome topology as a pervasive, yet
259 underappreciated, substrate of adaptive evolution. Together, our results establish
260 long-range genomic rearrangements as an important evolutionary force that has
261 repeatedly sculpted mammalian diversity.
262

263 Methods

264 Genome data

265 We obtained the chromosomal coordinates of human orthologous genes for 18
266 mammalian species from Ensembl (http://www.ensembl.org). Fifty three genomes
267 not represented in Ensemble were obtained from DNA Zoo

(https://www.dnazoo.org/assemblies) and Bat1K Project (https://bat1k.com/). We aligned the genome FASTA files to the human genome using LASTAL(https://github.com/lpryszcz/last). Resulting maf files were processed with *'last-split'* and converted to chain files using *'maf-convert'* utility (https://github.com/lpryszcz/last). To obtain orthologous genomic coordinates, we used the UCSC LiftOver tool (https://genome.ucsc.edu/cgi-bin/hgLiftOver). The phylogenetic tree of the species is given in the Figure S3. The genome assembly information is provided in Dataset S1.

Identification of clade-specific loss-of-synteny (LoS) events

To define evolutionary breakpoints of long-range genomic rearrangements, we used a distance-based approach. For each species, we first calculated linear distances between non-redundant all possible *cis* gene pairs. Gene pairs separated by ≤1 Mb were considered syntenic in a given species. The corresponding intergenic distances between orthologues of these syntenic pairs were then obtained for all other species and their distribution was visualized as histograms using the 'hist', function in R. The analysis revealed a bimodal distribution with two modes separated at around 10 Mb distance. This 10 Mb threshold was, therefore, used as a threshold to define loss of synteny events. Gene pairs that were within 1 mb distance in one species but exceeded 10Mb in other species were categorized as *cis*-rearrangement. If the orthologues of syntenic pairs were located on different chromosomes in another species, they were classified as *trans*-rearrangements. To minimize noise that might result from retro-transposition or assembly errors, we further obtained the set where the orthologous disruption occurred with at least 3 genes on either side of the break-point. We further calculated the inter-breakpoint distances defined as the linear distances between gene pairs forming breakpoints across all species. The distribution of distances suggested a distinct natural cut-off of 1.4 Mb (Figure S4), below which the breakpoints can be considered as clustered into evolutionary break-point region (EBRs). An EBR was identified as a clade-specific loss-of-synteny (LoS) event if it engages in LoS events in at least 50% of the species within a given mammalian clade, while being syntenic in most other clades (split in not more than two species).

301 **Phylogenetic comparative analyses of frequency of GRs**
302 We used mean frequency of GRs for each species and perform 'phenogram'
303 analysis using 'phytools' and DTT analysis using 'geiger' R-packges. We assumed
304 Brownian Motion (BM) model to simulate (*nsim=1000*) the evolution of GR
305 frequencies through time. The default average squared Euclidean distance was
306 used as metric.
307
308
309 **Gene Ontology analysis**
310 For each evolutionary breakpoint region (EBR), we extracted all genes within EBR
311 and 10 genes upstream and downstream of both ends. These unique gene sets
312 were compiled for each clade. Gene ontology (GO) enrichment analysis was
313 performed using the ToppFun function from the ToppGene Suite
314 (https://toppgene.cchmc.org/) to fetch the GO Biological Process categories. P-
315 values were corrected using Benjamini-Hoschberg method.
316
317 **Gene expression analysis**
318 We retrieved the expression data of CRHR1 and UGT1A1 of 35 human tissues from
319 the TissueEnrich database(https://tissueenrich.gdcb.iastate.edu/) for tissue specific
320 gene enrichment analysis. To calculate expression divergence, we used tissue-wide
321 expression data from the Bgee database(https://www.bgee.org/). For each gene
322 (CRHR1 and UGT1A1), a divergence ratio was calculated as the median of across-
323 clade versus within-clade distances. These gene-specific ratios were compared to
324 the genome-wide median divergence ratios calculated across all genes.
325
326 **Expression rate analysis**
327 We used 'TreeExp' R-package(https://github.com/hr1912/TreeExp) to evaluate the
328 evolutionary rates of expression divergence assuming Ornstein-Uhlenbeck model
329 of gene expression evolution. For each clade, we assigned a test species, a
330 reference species and an out-group species from phylogenetically adjacent clade.
331 We made three distance-based bins, each comprised of 25 genes, on either side of
332 the break-point. Gene expression data were obtained from Liu et al(Liu et al. 2023),
333 which provides expression profiles for three tissues: brain, kidney, and liver for

multiple species. For co-expression analysis, 10 genes on either side of breakpoint or the fusion point were obtained. Pearson's correlation coefficients across 26 mouse tissues (https://www.ncbi.nlm.nih.gov/sra/?term=srp020526) and 55 human tissues (https://gtexportal.org/home/) calculated for gene-sets around each reference point. Mean matrix of individual correlation matrices were plotted for visualization. Means of sliding windows of 3 genes along the diagonal of the correlation matrix was used for quantitative analysis.

Enhancer-promoter contact analysis

All human enhancer-promoter (EP) pairs and their orthologues in other species, were obtained from the dataset provided by Laverré et al(Laverré et al. 2022). The evolutionarily conserved EP pairs were then used to analyze disruption by clade-specific LoS events. If a conserved EP pair flanked a breakpoint unique to a clade, the pair was considered split by the rearrangement. For clades such as Chiroptera, Perissodactyla, Afrotheria, and the suborder Hystricomorpha, for which the enhancer orthologs were not included in the dataset by Laverré et al, the coordinates were lifted over using the UCSC liftOver tool (https://genome-store.ucsc.edu/). To calculate the statistical significance of observed EP pair disruptions, we performed bootstrap by randomizations breakpoint coordinates across the human genome 1000 times while keeping the chromosomal distribution of breakpoints same as original set. The bootstrap-based p-values were obtained using:

$$p = \frac{1}{B}\left(1 + \sum_{b=1}^{B} (1)_{k_b > k}\right)$$

where B is the total number of bootstrap samples, k is the observed number of disrupted EP pairs.

Hi-C analysis

We used HUGIn web browser (https://yunliweb.its.unc.edu/hugin/tutorial_page.php), to fetch virtual 4C interaction profiles at 40 kb resolution from human Hi-C data across relevant tissues. For mouse (mm10), .cool files were obtained from the 4D Nucleome Data Portal (https://data.4dnucleome.org/) and virtual 4C profiles were generated using Fit-Hi-C (https://github.com/ay-lab/fithic). We downloaded chromatin

compartment (A/B) files for both human and mouse tissues from the 4D Nucleome. Change in compartment along the genomic regions spanning the break-points was calculated using Kronecker's delta function:

$$\delta_{i\,j} \equiv \begin{cases} 0 & \text{for } i \neq j \\ 1 & \text{for } i = j. \end{cases}$$

If consecutive genomic bins i and j had same compartment (A-A or B-B), the function takes the value 1, and zero when i and j bins had different compartment values (A-B or B-A). We calculated the average and 95% confidence intervals of Kronecker's delta across all breakpoints for each tissue and clade (supplementary). For compact representation a global average of Kronecker's delta was plotted at 250 kb resolution around +/- 1 Mb to the break-point.

Linkage disequilibrium and recombination rates

LD scores from 1000 genomes and the recombination rates were obtained from Alkes group (https://zenodo.org/records/8182036) and Halldorsson et al(Halldorsson et al. 2019) respectively. The sliding means of these scores in 20kb bins around the reference points were plotted as a function of distance from the fusion-points.

The source of all datasets used are listed in Dataset S2.

Data availability

All data generated or analysed during this study are included in its supplementary dataset files.

Competing interest statement

The authors declare that they have no competing interests

Acknowledgements

Authors duly acknowledge the financial support from Department of Biotechnology, India (BT/PR40149/BTIS/137/36/2022, BT/PR40198/BTIS/137/56/2023). JB performed all the data analysis and prepared the figures. ML helped in coding. KSS conceived, improvised, guided, and wrote the manuscript.

Figure Legends

Figure 1. Mapping long-range genomic rearrangements across mammalian lineages. (a) Schematic representation of the strategy to map long-range genomic rearrangments. The distribution plot of genomic distance between adjacent genes in a species, which were <1 Mb apart in another species. Vertical line demarcates the separation of gene-pairs by >10mb in a species. **(b)** Heatmap representation of number of pair-wise long-range genomic rearrangements between lineages

Figure 2. Phylogenetic analysis of GR frequency. (a) Phenogram of mean GR frequency across mammals. The nodes and edges are coloured clade-wise. Ancestral nodes are inferred using Maximum Likelihood approach **(b)** Clade-wise Disparity-Through-Time (DTT) plots. The observed trait variations are coloured clade-wise. The expected variations (dark grey) are simulated assuming Brownian Motion model. Light grey curves represent the 95% confidence interval of simulated variations. **(c)** Clade-specific loss of synteny (LoS) events inferred using strategy given in the Methods section. Highlighted in rectangles are the clade-specific LoS events.

Figure 3. Functional associations of synteny disruptions. Enrichment of GO Biological Process terms among genes flanking the clade-specific EBRs. We implemented Benjamini-Hochberg correction of multiple testing. FDRs on the x-axis are converted to -log10 scale. The vertical lines mark the FDRs of 0.05.

Figure 4. Gene expression evolution around clade-specific breakpoints. **(a)** Overall strategy of expression rate analysis. Three consecutive genomic bins as function of distance from the clade-specific breakpoints were taken. Each bin contained 25 genes. Expression rates of genes each bin was calculated assuming Ornstein-Uhlenbeck model of transcriptome evolution. **(b)** Lineage-specific expression rates of the genes as a function of distance from the clade-specific evolutionary break-points. Each box represents the distribution of expression divergence values of 25 genes incrementally distant from the breakpoint. A species from the nearest order or sub-order was taken as reference species, while a species

429 hierarchically outside the clade of test and the reference species was taken as
430 outgroup species. P-values were calculated using Mann-Whitney U tests.
431
432 **Figure 5. Chromosomal position effect associated with the clade-specific loss**
433 **of synteny**. **(a)** Enrichment of clade-specific breakpoints within and around
434 enhancer-promoter loops in the species having syntenic configuration. Loop
435 coordinates were extended either side by half of the loop length-L. **(b)** The number of
436 conserved enhancer-promoter contacts that had lost proximity through GR in a
437 clade-specific manner, superimposed onto the random null distribution obtained from
438 controlled randomized of breakpoints. P-values are calculated using bootstrap
439 method. Shown are the plots for the cumulated set and the clade-specific sets. **(c)**
440 Kronecker's δ_{ij}, signifying change in A and B compartment states of neighbouring
441 domains, as a function of distance from the break-points in primates and rodents.
442 Drop in Kronecker's delta signifies the switch in states (A-to-B or B-to-A). The three
443 plots correspond to syntenic configuration in mouse (left), distal regions (syntenic in
444 human) when juxtaposed in mouse (middle), rearranged syntenic regions in human
445 (right) respectively in case of primate-specific LoS. Similarly, for rodent-specific LoS,
446 syntenic configuration in human (left), distal juxtaposed regions in human (middle)
447 and rearranged syntenic regions in mouse (right) are plotted. **(d)** Chromatin
448 compartment states (leading Eigen vector of Hi-C contact matrix) for regions around
449 TAC1 locus, which exhibited primate-specific LoS nearby, in mouse and human
450 neuronal cells. A and B compartments are coloured as red and grey colours
451 respectively.
452
453 **Figure 6. Illustrative examples of clade-specific breakpoints. (a-b)** Left-panels:
454 CRHR1 and UGT1A expression values in 35 human tissues respectively. Right-
455 panels: expression divergence calculated as the Euclidean distance across tissues
456 and summarized as ratio of across-clade to within-clade distances. **(b-c)** Mouse-to-
457 human and human-to-cow synteny plots around (b) CRHR1, and (c) UGT1A gene
458 respectively. Shown below are the tracks of RefSeq non-redundant genes, H3K27ac
459 modification, and virtual 4C in relevant tissues. The clade-specific break-point
460 regions are highlighted by vertical bars. 4C reference loci are highlighted using
461 arrow-heads. Black and red curves represent observed and expected 4C signals

462 respectively. Green curve represents -log10 of p-values. Blue dashed line represents
463 the p-value cut-off of 0.05. Red arcs mark the significantly frequent chromatin
464 contacts.
465
466 **Figure 7. Signatures of selective constraints**. **(a)** Human LD score and **(b)**
467 recombination rates around the fusion points resulting from primate-specific LoS
468 events. **(c)** Distribution of number of primates exhibiting evolutionarily fixed
469 configuration of rearranged genomic regions. **(d)** Mean co-expression of genes
470 around primate-specific breakpoints in mouse (top panel) and around rearranged
471 fusion points in human (middle panel). Bottom panel shows sliding means of the
472 values around diagonal of the co-expression matrices of mouse and human. P-
473 values were calculated using two-tailed unpaired t-tests.
474

475 ## References:

476 Akhtar W, de Jong J, Pindyurin A V, Pagie L, Meuleman W, de Ridder J, Berns A, Wessels LFA,
477 van Lohuizen M, van Steensel B. 2013. Chromatin position effects assayed by
478 thousands of reporters integrated in parallel. *Cell* 154:914–927.
479 Bagadia M, Chandradoss KR, Jain Y, Singh H, Lal M, Sandhu KS. 2019. Evolutionary Loss of
480 Genomic Proximity to Conserved Noncoding Elements Impacted the Gene Expression
481 Dynamics During Mammalian Brain Development. *Genetics* [Internet] 211:1239–1254.
482 Available from: http://www.ncbi.nlm.nih.gov/pubmed/30796012
483 Bedell MA, Brannan CI, Evans EP, Copeland NG, Jenkins NA, Donovan PJ. 1995. DNA
484 rearrangements located over 100 kb 5' of the Steel (Sl)-coding region in Steel-panda
485 and Steel-contrasted mice deregulate Sl expression and cause female sterility by
486 disrupting ovarian follicle development. *Genes Dev.* 9:455–470.
487 Benjamin A, Costa AN Da, Delaunois A, Rosseels ML, Valentin JP. 2015. Renal safety
488 pharmacology in drug discovery and development. *Handb. Exp. Pharmacol.* 229.
489 Bittner NKJ, Mack KL, Nachman MW. 2021. Gene expression plasticity and desert adaptation
490 in house mice*. *Evolution (N. Y).* 75.
491 Bozek K, Wei Y, Yan Z, Liu X, Xiong J, Sugimoto M, Tomita M, Pääbo S, Sherwood CC, Hof PR,
492 et al. 2015. Organization and Evolution of Brain Lipidome Revealed by Large-Scale
493 Analysis of Human, Chimpanzee, Macaque, and Mouse Tissues. *Neuron* 85.

494 Chen X, Zhang J. 2016. The Genomic Landscape of Position Effects on Protein Expression
495 Level and Noise in Yeast. *Cell Syst.* 2:347–354.
496 Chiang C, Scott AJ, Davis JR, Tsang EK, Li X, Kim Y, Hadzic T, Damani FN, Ganel L, GTEx
497 Consortium, et al. 2017. The impact of structural variation on human gene expression.
498 *Nat. Genet.* 49:692–699.
499 De S, Teichmann SA, Babu MM. 2009. The impact of genomic neighborhood on the
500 evolution of human and chimpanzee transcriptome. *Genome Res.* 19:785–794.
501 Derous D, Sahu J, Douglas A, Lusseau D, Wenzel M. 2021. Comparative genomics of
502 cetartiodactyla: Energy metabolism underpins the transition to an aquatic lifestyle.
503 *Conserv. Physiol.* 9.
504 Dickinson H, Moritz K, Wintour EM, Walker DW, Kett MM. 2007. A comparative study of
505 renal function in the desert-adapted spiny mouse and the laboratory-adapted C57BL/6
506 mouse: Response to dietary salt load. *Am. J. Physiol. - Ren. Physiol.* 293.
507 Diessler M, Ventureira M, Hernandez R, Sobarzo C, Casas L, Barbeito C, Cebral E. 2017.
508 Differential expression and activity of matrix metalloproteinases 2 and 9 in canine early
509 placenta. *Reprod. Domest. Anim.* 52.
510 Doherty A, de Magalhães JP. 2016. Has gene duplication impacted the evolution of
511 Eutherian longevity? *Aging Cell* 15.
512 Dunn-Fletcher CE, Muglia LM, Pavlicev M, Wolf G, Sun MA, Hu YC, Huffman E, Tumukuntala
513 S, Thiele K, Mukherjee A, et al. 2018. Anthropoid primate–specific retroviral element
514 THE1B controls expression of CRH in placenta and alters gestation length. *PLoS Biol.* 16.
515 Elgin SC, Reuter G. 2013. Position-effect variegation, heterochromatin formation, and gene
516 silencing in Drosophila. *Cold Spring Harb Perspect Biol* [Internet] 5:a017780. Available
517 from: http://www.ncbi.nlm.nih.gov/pubmed/23906716
518 Fantes J, Redeker B, Breen M, Boyle S, Brown J, Fletcher J, Jones S, Bickmore W, Fukushima
519 Y, Mannens M, et al. 1995. Aniridia-associated cytogenetic rearrangements suggest
520 that a position effect may cause the mutant phenotype. *Hum. Mol. Genet.* 4:415–422.
521 Flomen RH, Vatcheva R, Gorman PA, Baptista PR, Groet J, Barišić I, Ligutic I, Nižetić D. 1998.
522 Construction and Analysis of a Sequence-Ready Map in 4q25: Rieger Syndrome Can Be
523 Caused by Haploinsufficiency ofRIEG, but Also by Chromosome Breaks ≈90 kb
524 Upstream of This Gene. *Genomics* 47:409–413.
525 Gbadegesin RA, Hall G, Adeyemo A, Hanke N, Tossidou I, Burchette J, Wu G, Homstad A,

526 Sparks MA, Gomez J, et al. 2014. Mutations in the gene that encodes the F-Actin
527 binding protein anillin cause FSGS. *J. Am. Soc. Nephrol.* 25.
528 Guntawang T, Sittisak T, Kochagul V, Srivorakul S, Photichai K, Boonsri K, Janyamethakul T,
529 Boonprasert K, Langkaphin W, Thitaram C, et al. 2021. Pathogenesis of hemorrhagic
530 disease caused by elephant endotheliotropic herpesvirus (EEHV) in Asian elephants
531 (Elephas maximus). *Sci. Rep.* 11.
532 Halldorsson B V., Palsson G, Stefansson OA, Jonsson H, Hardarson MT, Eggertsson HP,
533 Gunnarsson B, Oddsson A, Halldorsson GH, Zink F, et al. 2019. Human genetics:
534 Characterizing mutagenic effects of recombination through a sequence-level genetic
535 map. *Science (80-.).* 363.
536 Hudson NJ, Baker ML, Hart NS, Wynne JW, Gu Q, Huang Z, Zhang G, Ingham AB, Wang L,
537 Reverter A. 2014. Sensory rewiring in an echolocator: Genome-wide modification of
538 retinogenic and auditory genes in the bat Myotis davidii. *G3 Genes, Genomes, Genet.* 4.
539 Jebb D, Huang Z, Pippel M, Hughes GM, Lavrichenko K, Devanna P, Winkler S, Jermiin LS,
540 Skirmuntt EC, Katzourakis A, et al. 2020. Six reference-quality genomes reveal evolution
541 of bat adaptations. *Nature* 583.
542 Jezova D, Ochedalski T, Glickman M, Kiss A, Aguilera G. 1999. Central corticotropin-releasing
543 hormone receptors modulate hypothalamic- pituitary-adrenocortical and
544 sympathoadrenal activity during stress. *Neuroscience* 94.
545 Jiang Y, Xie M, Chen W, Talbot R, Maddox JF, Faraut T, Wu C, Muzny DM, Li Y, Zhang W, et
546 al. 2014. The sheep genome illuminates biology of the rumen and lipid metabolism.
547 *Science (80-.).* 344.
548 Kawai YK, Sano K, Ikenaka Y, Nakayama SMM, Kondo M, Kubota A, Ishizuka M. 2021.
549 Evolutionary history of mammalian UDP-glucuronosyltransferase (UGT)1 and UGT2
550 families: the emergence of UGT2B subfamily in eutherians after the diversification of
551 flowering plants. *bioRxiv*.
552 Kim J, Farré M, Auvil L, Capitanu B, Larkin DM, Ma J, Lewin HA. 2017. Reconstruction and
553 evolutionary history of eutherian chromosomes. *Proc. Natl. Acad. Sci. U. S. A.*
554 114:E5379–E5388.
555 Kleinjan DJ, Van Heyningen V. 1998. Position effect in human genetic disease. *Hum. Mol.*
556 *Genet.* 7.
557 Krebs I. 1997. Translocation breakpoint maps 5 kb 3’ from TWIST in a patient affected with

558 Saethre-Chotzen syndrome. *Hum. Mol. Genet.* 6:1079–1086.
559 Laverré A, Tannier E, Necsulea A. 2022. Long-range promoter–enhancer contacts are
560 conserved during evolution and contribute to gene expression robustness. *Genome*
561 *Res.* 32.
562 Lewis JH. 1974. Comparative hematology: Studies on elephants, Elephas maximus. *Comp.*
563 *Biochem. Physiol. -- Part A Physiol.* 49.
564 Liu W, Zhu P, Li Meng, Li Z, Yu Y, Liu G, Du J, Wang X, Yang J, Tian R, et al. 2023. Large-scale
565 across species transcriptomic analysis identifies genetic selection signatures associated
566 with longevity in mammals. *EMBO J.* 42.
567 Luo H, Arndt W, Zhang Y, Shi G, Alekseyev MA, Tang J, Hughes AL, Friedman R. 2012.
568 Phylogenetic analysis of genome rearrangements among five mammalian orders. *Mol.*
569 *Phylogenet. Evol.* 65:871–882.
570 Milot E, Fraser P, Grosveld F. 1996. Position effects and genetic disease. *Trends Genet.* 12.
571 Muntané G, Horvath JE, Hof PR, Ely JJ, Hopkins WD, Raghanti MA, Lewandowski AH, Wray
572 GA, Sherwood CC. 2015. Analysis of synaptic gene expression in the neocortex of
573 primates reveals evolutionary changes in glutamatergic neurotransmission. *Cereb.*
574 *Cortex* 25.
575 Nishibori Y, Katayama K, Parikka M, Oddsson Á, Nukui M, Hultenby K, Wernerson A, He B,
576 Ebarasi L, Raschperger E, et al. 2011. Glcci1 deficiency leads to proteinuria. *J. Am. Soc.*
577 *Nephrol.* 22.
578 Pays E. 2021. The function of apolipoproteins L (APOLs): relevance for kidney disease,
579 neurotransmission disorders, cancer and viral infection. *FEBS J.* 288.
580 Poole DC, Erickson HH. 2011. Highly athletic terrestrial mammals: Horses and dogs. *Compr.*
581 *Physiol.* 1.
582 Pusey A, Williams J, Goodall J. 1997. The influence of dominance rank on the reproductive
583 success of female chimpanzees. *Science (80-.).* 277.
584 Real FM, Haas SA, Franchini P, Xiong P, Simakov O, Kuhl H, Schöpflin R, Heller D,
585 Moeinzadeh MH, Heinrich V, et al. 2020. The mole genome reveals regulatory
586 rearrangements associated with adaptive intersexuality. *Science (80-.).* 370.
587 Roth LS V, McGreevy P. 2025. Horse vision through two lenses: Tinbergen's Four Questions
588 and the Five Domains. *Front. Vet. Sci.* 12:1647911.
589 Sapolsky RM. 2021. Glucocorticoids, the evolution of the stress-response, and the primate

590 predicament. *Neurobiol. Stress* 14.
591 Savage VM, Allen AP, Brown JH, Gillooly JF, Herman AB, Woodruff WH, West GB. 2007.
592 Scaling of number, size, and metabolic rate of cells with body size in mammals. *Proc.*
593 *Natl. Acad. Sci. U. S. A.* 104.
594 Singh A, Bagadia M, Sandhu KS. 2016. Spatially coordinated replication and minimization of
595 expression noise constrain three-dimensional organization of yeast genome. *DNA Res*
596 [Internet] 23:155–169. Available from:
597 http://www.ncbi.nlm.nih.gov/pubmed/26932984
598 Smith R, Nicholson RC. 2007. Corticotrophin releasing hormone and the timing of birth.
599 *Front. Biosci.* 12.
600 Spanaki C, Sidiropoulou K, Petraki Z, Diskos K, Konstantoudaki X, Volitaki E, Mylonaki K,
601 Savvaki M, Plaitakis A. 2024. Glutamate-specific gene linked to human brain evolution
602 enhances synaptic plasticity and cognitive processes. *iScience* 27.
603 Sulak M, Fong L, Mika K, Chigurupati S, Yon L, Mongan NP, Emes RD, Lynch VJ. 2016. TP53
604 copy number expansion is associated with the evolution of increased body size and an
605 enhanced DNA damage response in elephants. *Elife* [Internet] 5. Available from:
606 http://www.ncbi.nlm.nih.gov/pubmed/27642012
607 Tomas NM, Beck LH, Meyer-Schwesinger C, Seitz-Polski B, Ma H, Zahner G, Dolla G, Hoxha E,
608 Helmchen U, Dabert-Gay A-S, et al. 2014. Thrombospondin Type-1 Domain-Containing
609 7A in Idiopathic Membranous Nephropathy. *N. Engl. J. Med.* 371.
610 Wallrath LL, Elgin SC. 1995. Position effect variegation in Drosophila is associated with an
611 altered chromatin structure. *Genes Dev* [Internet] 9:1263–1277. Available from:
612 http://www.ncbi.nlm.nih.gov/pubmed/7758950
613 Wang H, Zhao H, Sun K, Huang X, Jin L, Feng J. 2019. Evolutionary Basis of High-Frequency
614 Hearing in the Cochleae of Echolocators Revealed by Comparative Genomics. *Genome*
615 *Biol. Evol.* 12.
616 Wirth J, Wagner T, Meyer J, Pfeiffer RA, Tietze H-U, Schempp W, Scherer G. 1996.
617 Translocation breakpoints in three patients with campomelic dysplasia and autosomal
618 sex reversal map more than 130 kb from SOX9. *Hum. Genet.* 97:186–193.
619 Wooding FBP, Burton GJ. 2008. Comparative placentation: Structures, functions and
620 evolution.
621 Xu Z, Lee D-S, Chandran S, Le VT, Bump R, Yasis J, Dallarda S, Marcotte S, Clock B, Haghani N,

622 et al. 2022. Structural variants drive context-dependent oncogene activation in cancer.
623 *Nature* 612:564–572.
624 Zheng J, Erzurumluoglu AM, Elsworth BL, Kemp JP, Howe L, Haycock PC, Hemani G, Tansey
625 K, Laurin C, Pourcain BS, et al. 2017. LD Hub: A centralized database and web interface
626 to perform LD score regression that maximizes the potential of summary level GWAS
627 data for SNP heritability and genetic correlation analysis. *Bioinformatics* 33.
628

a

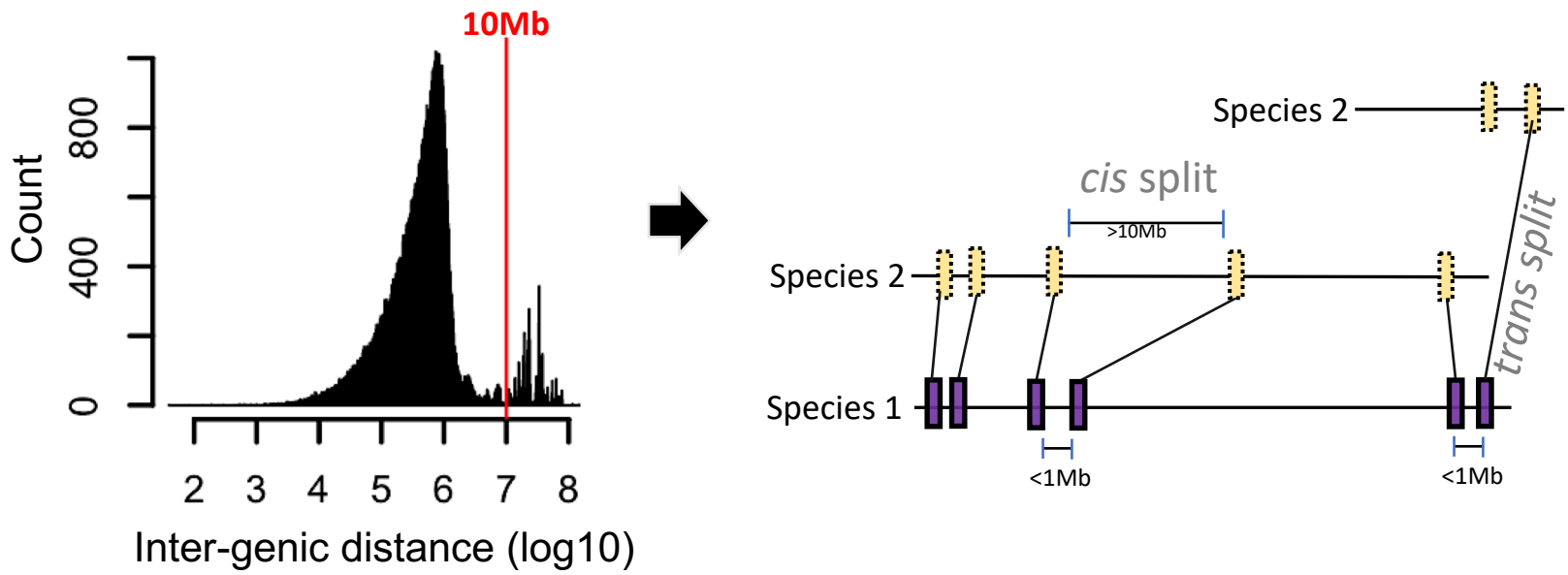
10Mb
Count
0
400
800
2
3
4
5
6
7
8
Inter-genic distance (log10)
Species 2
cis split
>10Mb
Species 2
Species 1
trans split
<1Mb
<1Mb

b

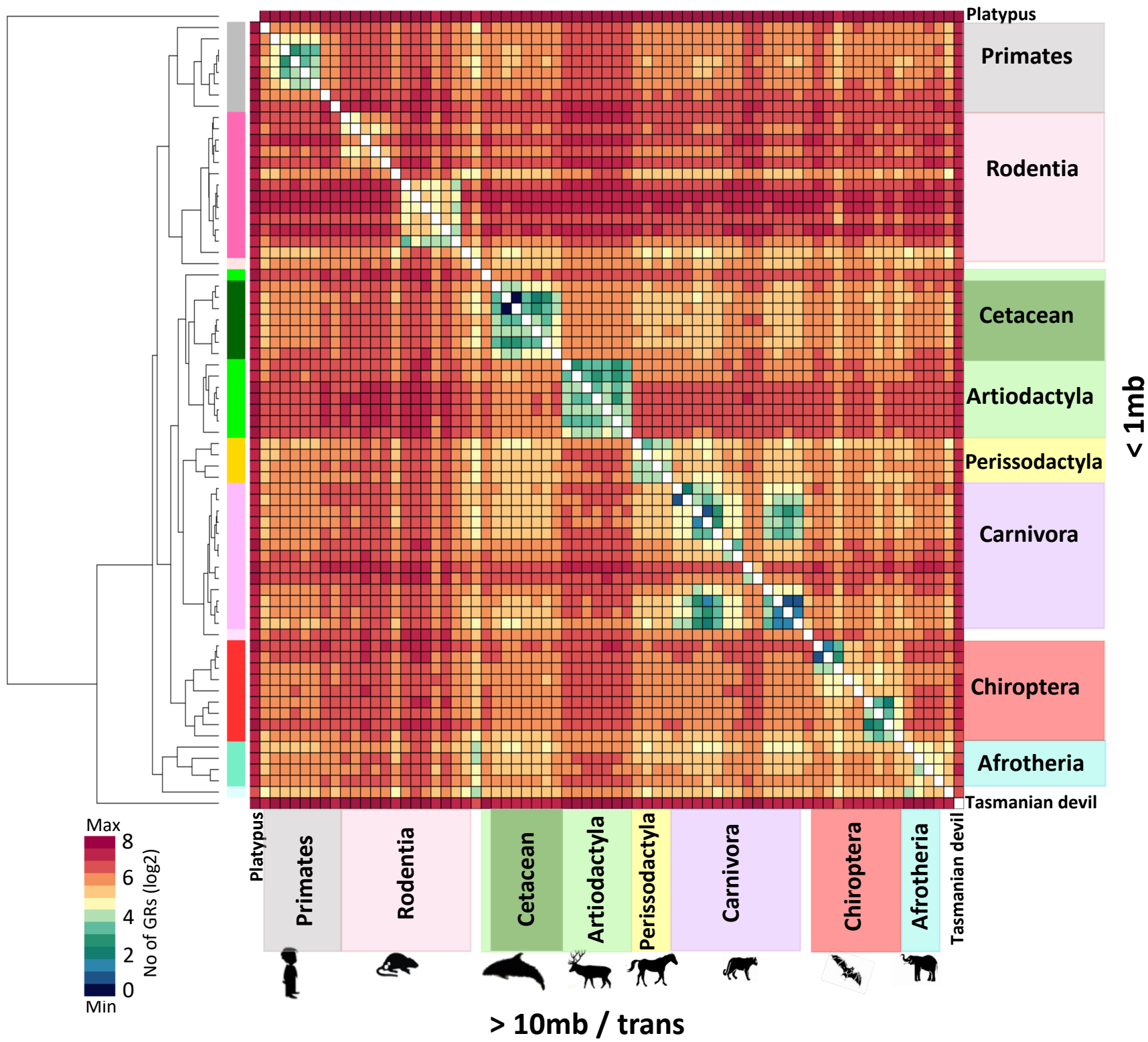
Platypus
Primates
Rodentia
Cetacean
Artiodactyla
Perissodactyla
Carnivora
Chiroptera
Afrotheria
Tasmanian devil
< 1mb
Max
8
6
4
2
0
Min
No of GRs (log2)
Platypus
Primates
Rodentia
Cetacean
Artiodactyla
Perissodactyla
Carnivora
Chiroptera
Afrotheria
Tasmanian devil
> 10mb / trans

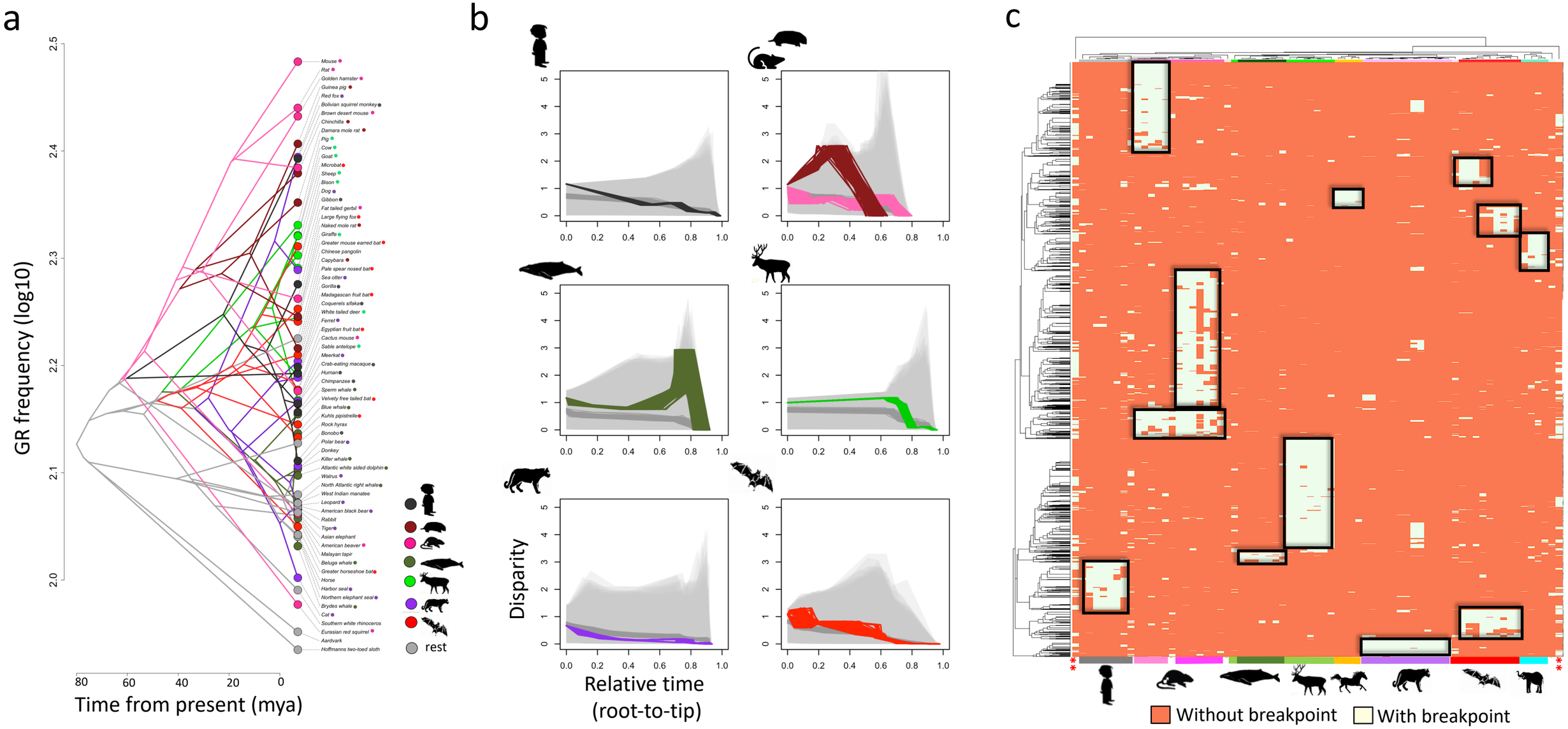
a
GR frequency (log10)
2.5
2.4
2.3
2.2
2.1
2.0
Mouse
Rat
Golden hamster
Guinea pig
Red fox
Bolivian squirrel monkey
Brown desert mouse
Chinchilla
Damara mole rat
Pig
Cow
Goat
Microbat
Sheep
Bison
Dog
Gibbon
Fat tailed gerbil
Large flying fox
Naked mole rat
Giraffe
Greater mouse eared bat
Chinese pangolin
Capybara
Pale spear nosed bat
Sea otter
Gorilla
Madagascan fruit bat
Coquerels sifaka
White tailed deer
Ferret
Egyptian fruit bat
Cactus mouse
Sable antelope
Meerkat
Crab-eating macaque
Human
Chimpanzee
Sperm whale
Velvety free tailed bat
Blue whale
Kuhls pipistrelle
Rock hyrax
Bonobo
Polar bear
Donkey
Killer whale
Atlantic white sided dolphin
Walrus
North Atlantic right whale
West Indian manatee
Leopard
American black bear
Rabbit
Tiger
Asian elephant
American beaver
Malayan tapir
Beluga whale
Greater horseshoe bat
Horse
Harbor seal
Northern elephant seal
Brydes whale
Cat
Southern white rhinoceros
Eurasian red squirrel
Aardvark
Hoffmanns two-toed sloth
rest
80
60
40
20
0
Time from present (mya)
b
Disparity
0.0
0.2
0.4
0.6
0.8
1.0
Relative time
(root-to-tip)
c
Without breakpoint
With breakpoint

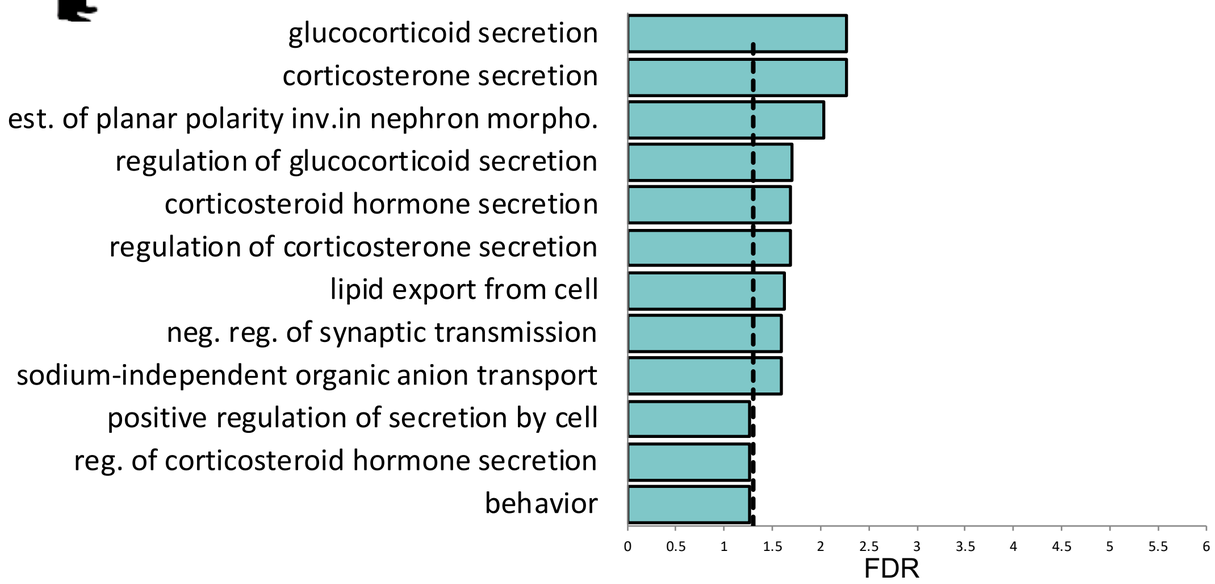
glucocorticoid secretion
corticosterone secretion
est. of planar polarity inv.in nephron morpho.
regulation of glucocorticoid secretion
corticosteroid hormone secretion
regulation of corticosterone secretion
lipid export from cell
neg. reg. of synaptic transmission
sodium-independent organic anion transport
positive regulation of secretion by cell
reg. of corticosteroid hormone secretion
behavior
0 0.5 1 1.5 2 2.5 3 3.5 4 4.5 5 5.5 6
FDR

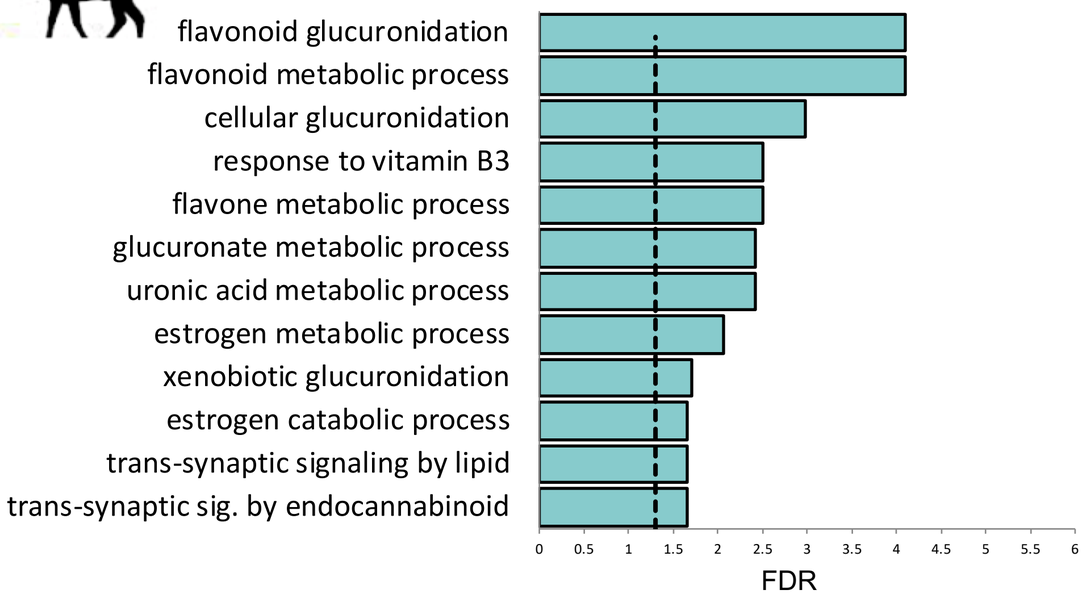
flavonoid glucuronidation
flavonoid metabolic process
cellular glucuronidation
response to vitamin B3
flavone metabolic process
glucuronate metabolic process
uronic acid metabolic process
estrogen metabolic process
xenobiotic glucuronidation
estrogen catabolic process
trans-synaptic signaling by lipid
trans-synaptic sig. by endocannabinoid
0 0.5 1 1.5 2 2.5 3 3.5 4 4.5 5 5.5 6
FDR

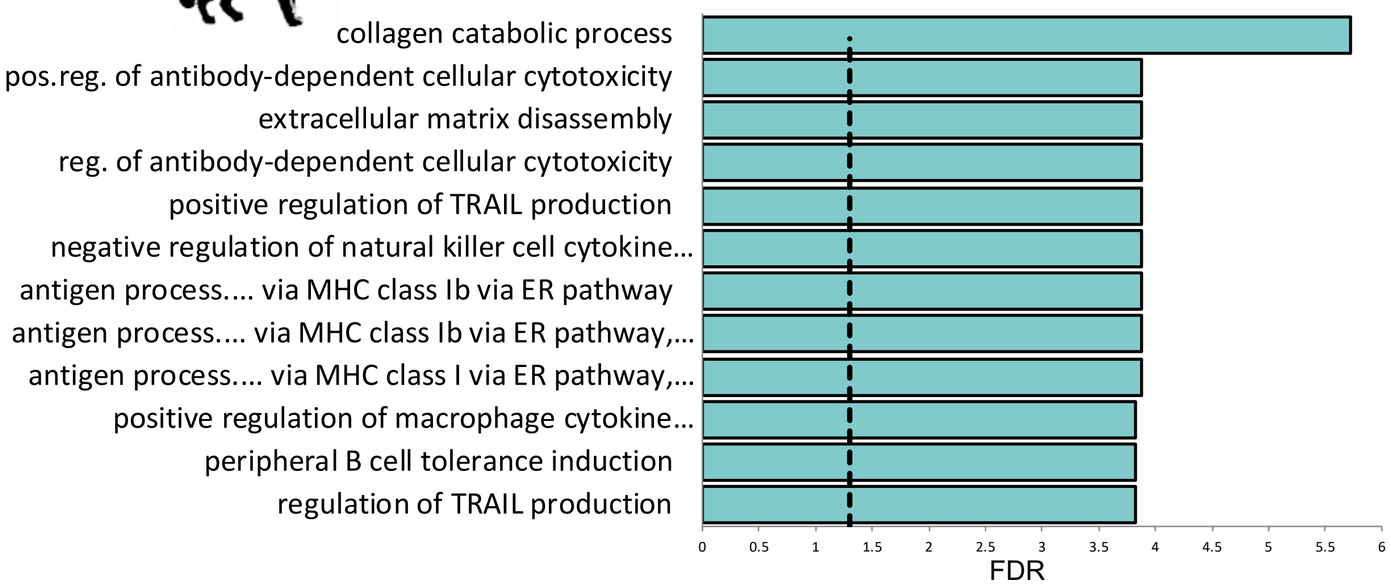
collagen catabolic process
pos.reg. of antibody-dependent cellular cytotoxicity
extracellular matrix disassembly
reg. of antibody-dependent cellular cytotoxicity
positive regulation of TRAIL production
negative regulation of natural killer cell cytokine...
antigen process.... via MHC class Ib via ER pathway
antigen process.... via MHC class Ib via ER pathway,...
antigen process.... via MHC class I via ER pathway,...
positive regulation of macrophage cytokine...
peripheral B cell tolerance induction
regulation of TRAIL production
0 0.5 1 1.5 2 2.5 3 3.5 4 4.5 5 5.5 6
FDR

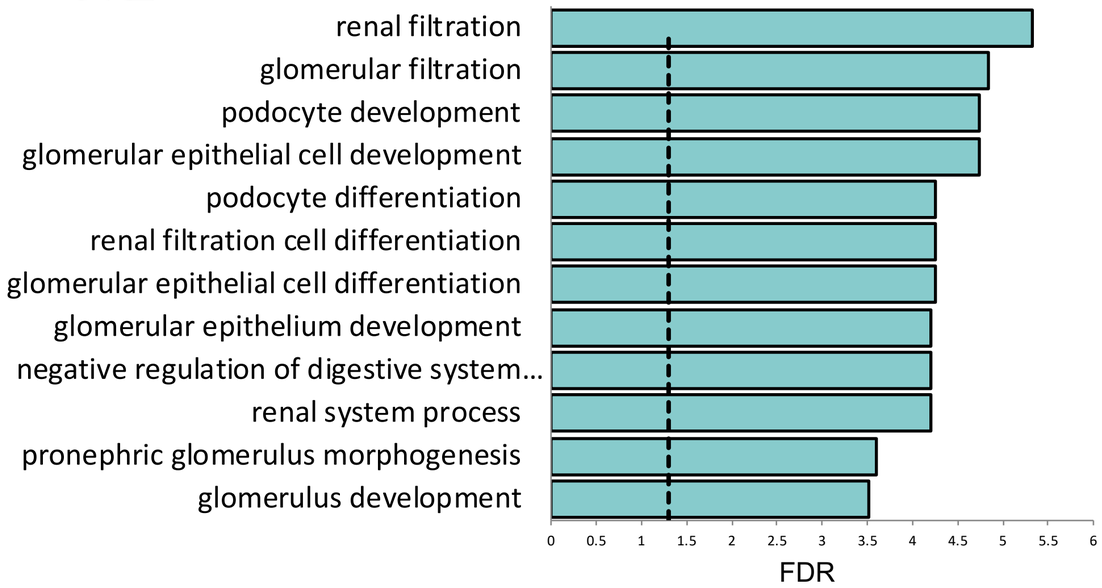
renal filtration
glomerular filtration
podocyte development
glomerular epithelial cell development
podocyte differentiation
renal filtration cell differentiation
glomerular epithelial cell differentiation
glomerular epithelium development
negative regulation of digestive system...
renal system process
pronephric glomerulus morphogenesis
glomerulus development
0 0.5 1 1.5 2 2.5 3 3.5 4 4.5 5 5.5 6
FDR

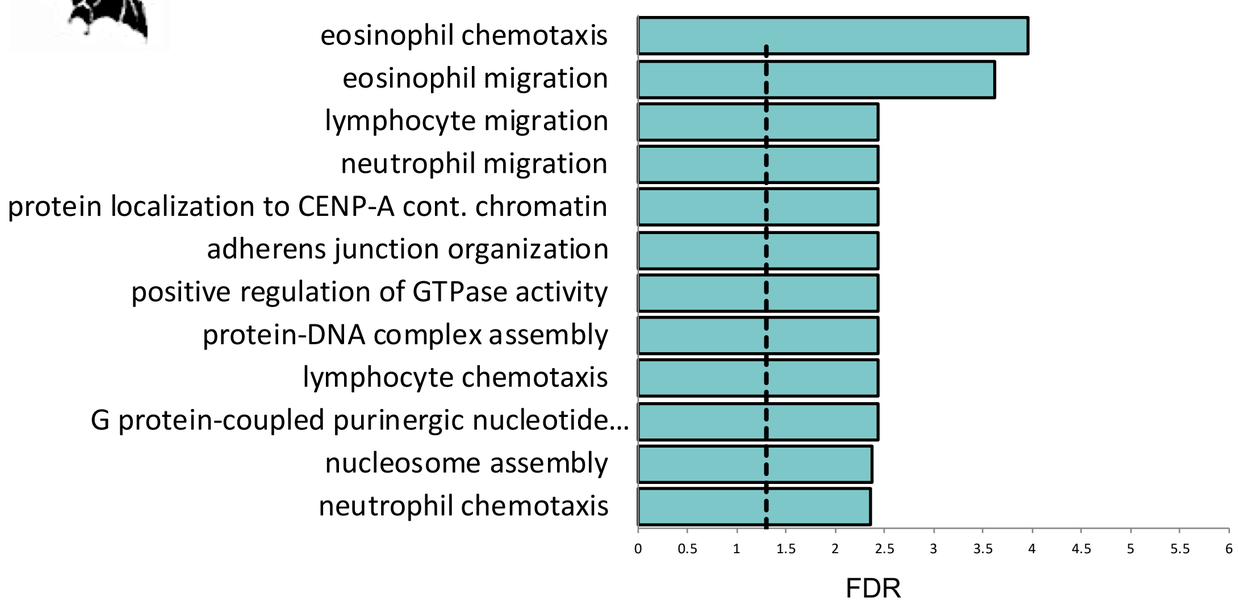
eosinophil chemotaxis
eosinophil migration
lymphocyte migration
neutrophil migration
protein localization to CENP-A cont. chromatin
adherens junction organization
positive regulation of GTPase activity
protein-DNA complex assembly
lymphocyte chemotaxis
G protein-coupled purinergic nucleotide...
nucleosome assembly
neutrophil chemotaxis
0 0.5 1 1.5 2 2.5 3 3.5 4 4.5 5 5.5 6
FDR

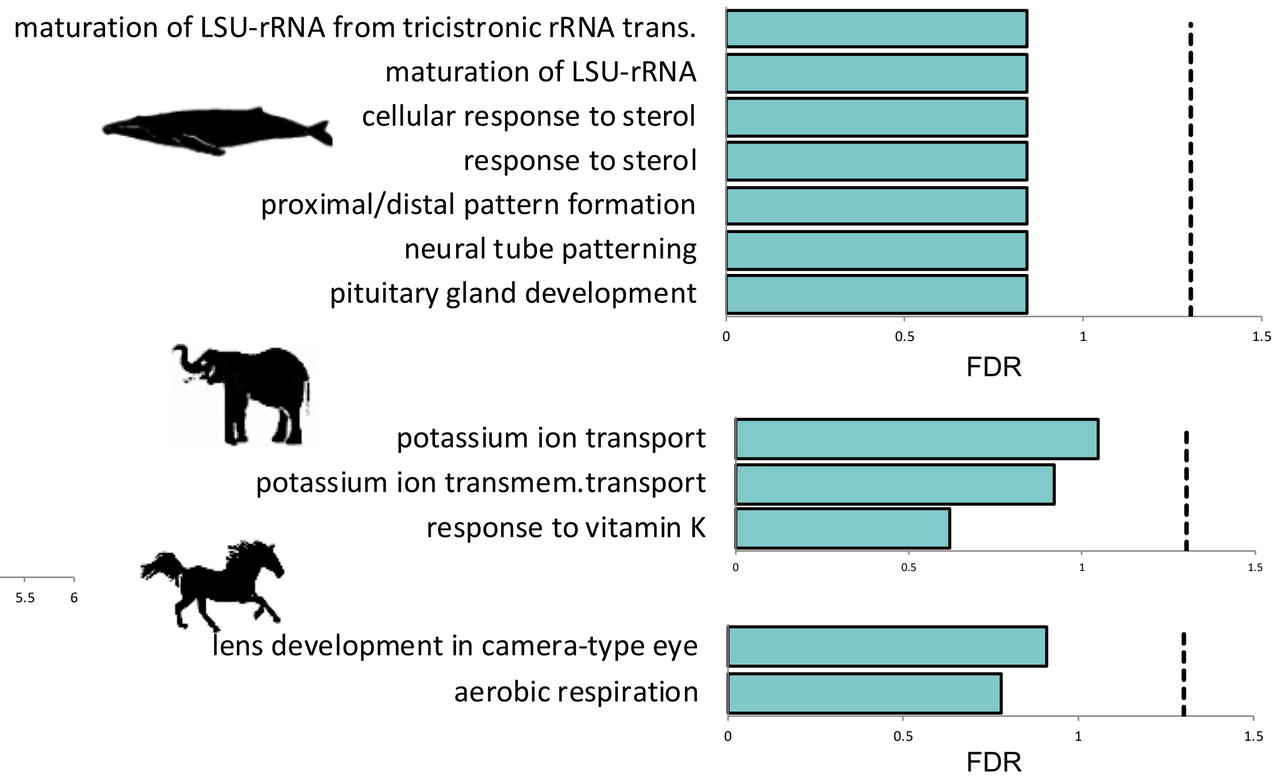
maturation of LSU-rRNA from tricistronic rRNA trans.
maturation of LSU-rRNA
cellular response to sterol
response to sterol
proximal/distal pattern formation
neural tube patterning
pituitary gland development
0 0.5 1 1.5
FDR
potassium ion transport
potassium ion transmem.transport
response to vitamin K
0 0.5 1 1.5
lens development in camera-type eye
aerobic respiration
0 0.5 1 1.5
FDR

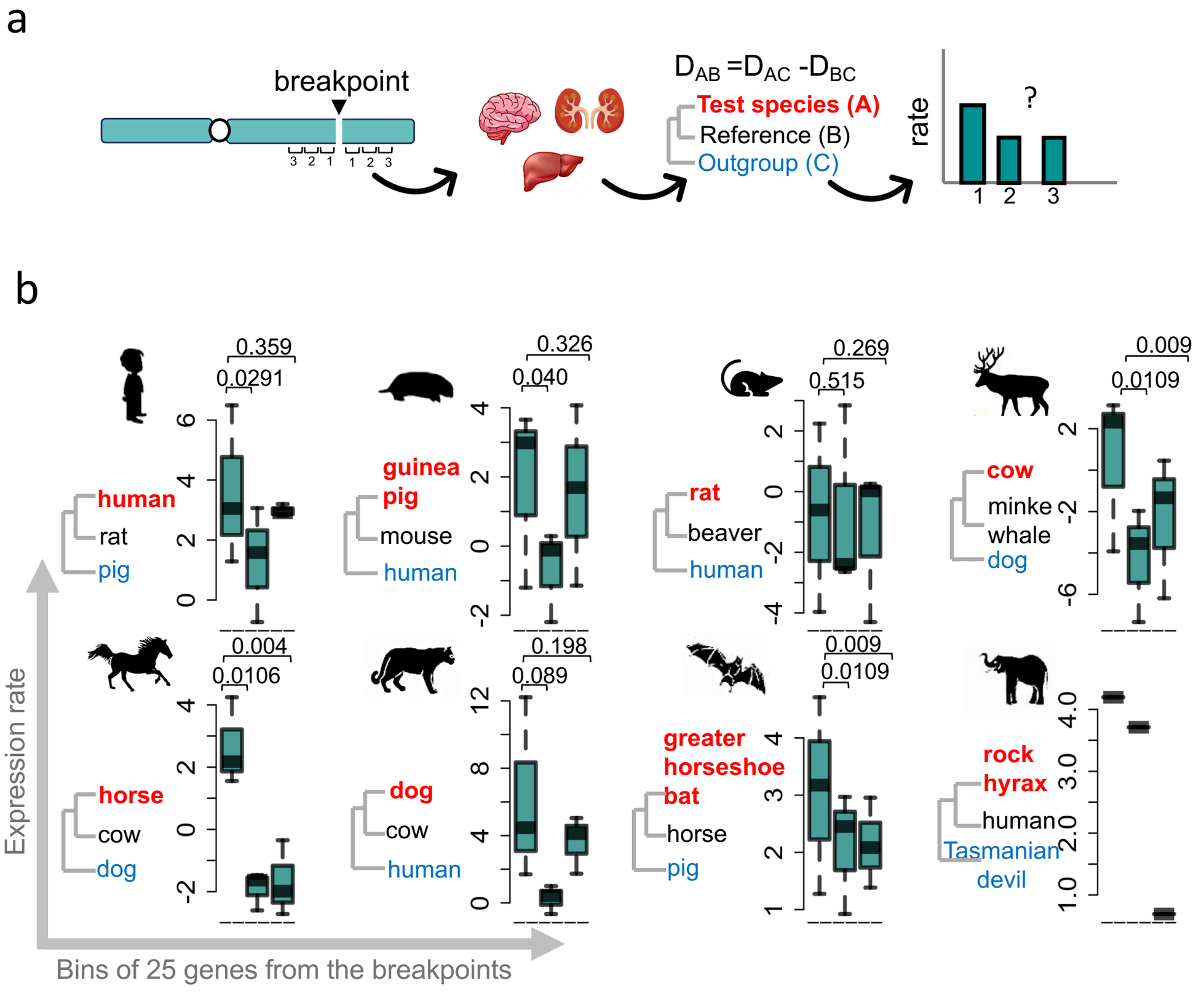
a
breakpoint
3 2 1 1 2 3
$D_{AB} = D_{AC} - D_{BC}$
Test species (A)
Reference (B)
Outgroup (C)
rate
?
1 2 3
b
0.359
0.0291
human
rat
pig
0.326
0.040
guinea pig
mouse
human
0.269
0.515
rat
beaver
human
0.009
0.0109
cow
minke whale
dog
0.004
0.0106
horse
cow
dog
0.198
0.089
dog
cow
human
0.009
0.0109
greater horseshoe bat
horse
pig
rock hyrax
human
Tasmanian devil
Expression rate
Bins of 25 genes from the breakpoints

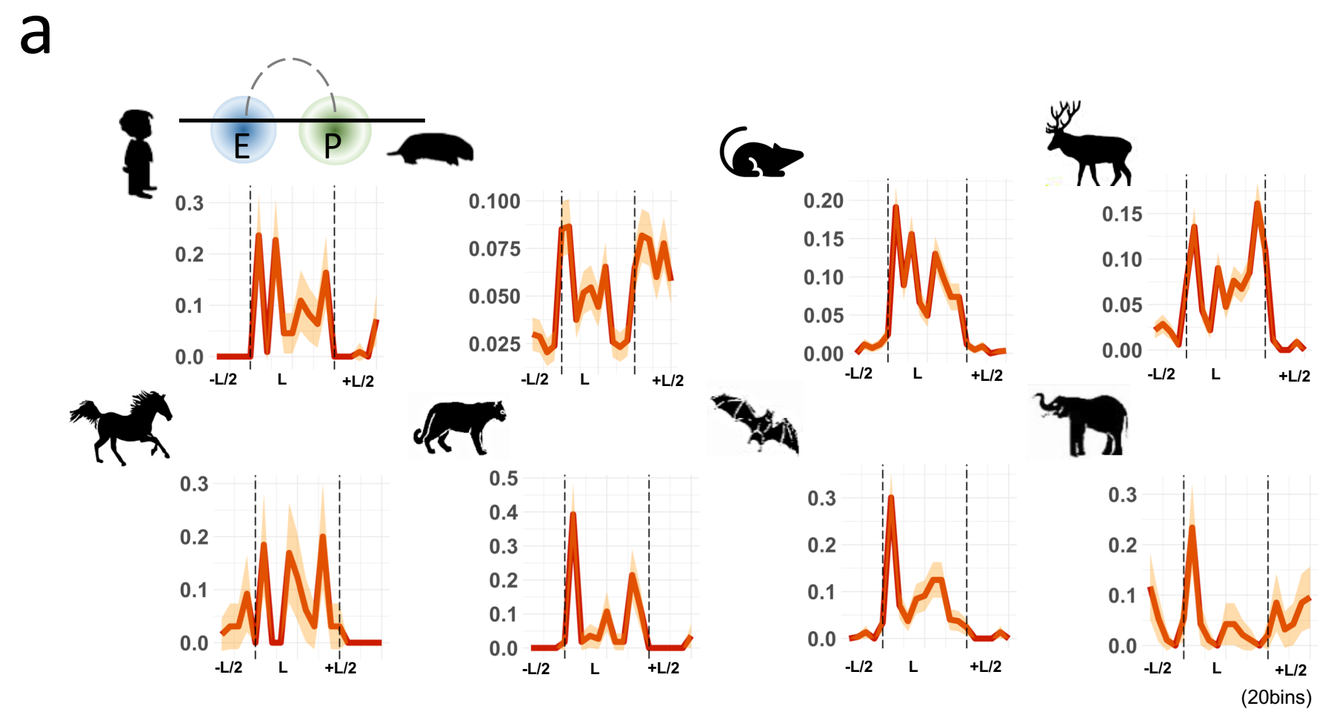
a
E
P
-L/2
L
+L/2
(20bins)

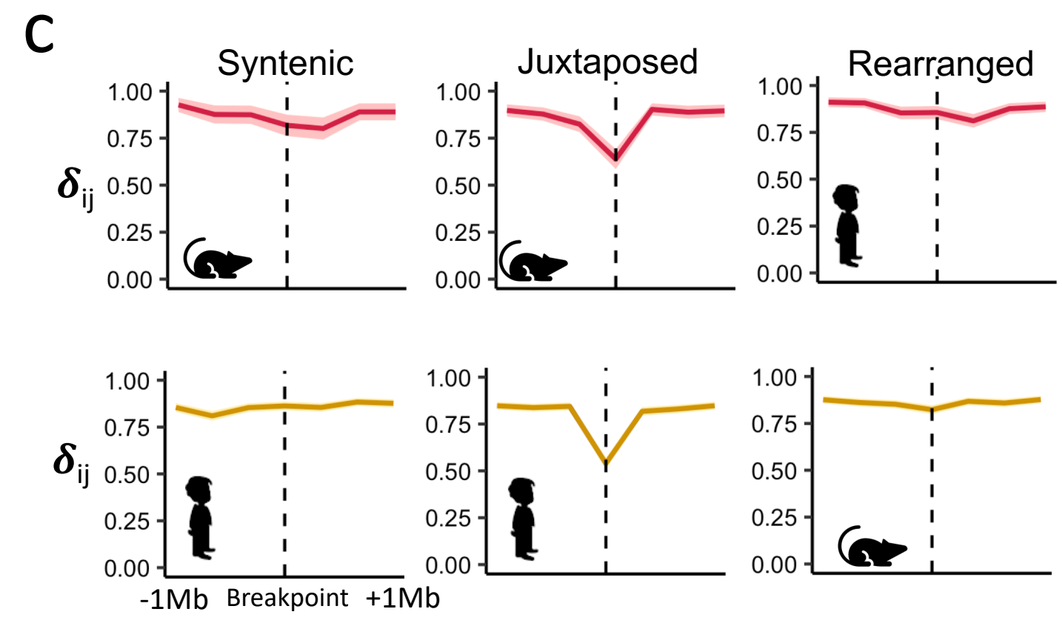
c
Syntenic
Juxtaposed
Rearranged
δij
-1Mb
Breakpoint
+1Mb

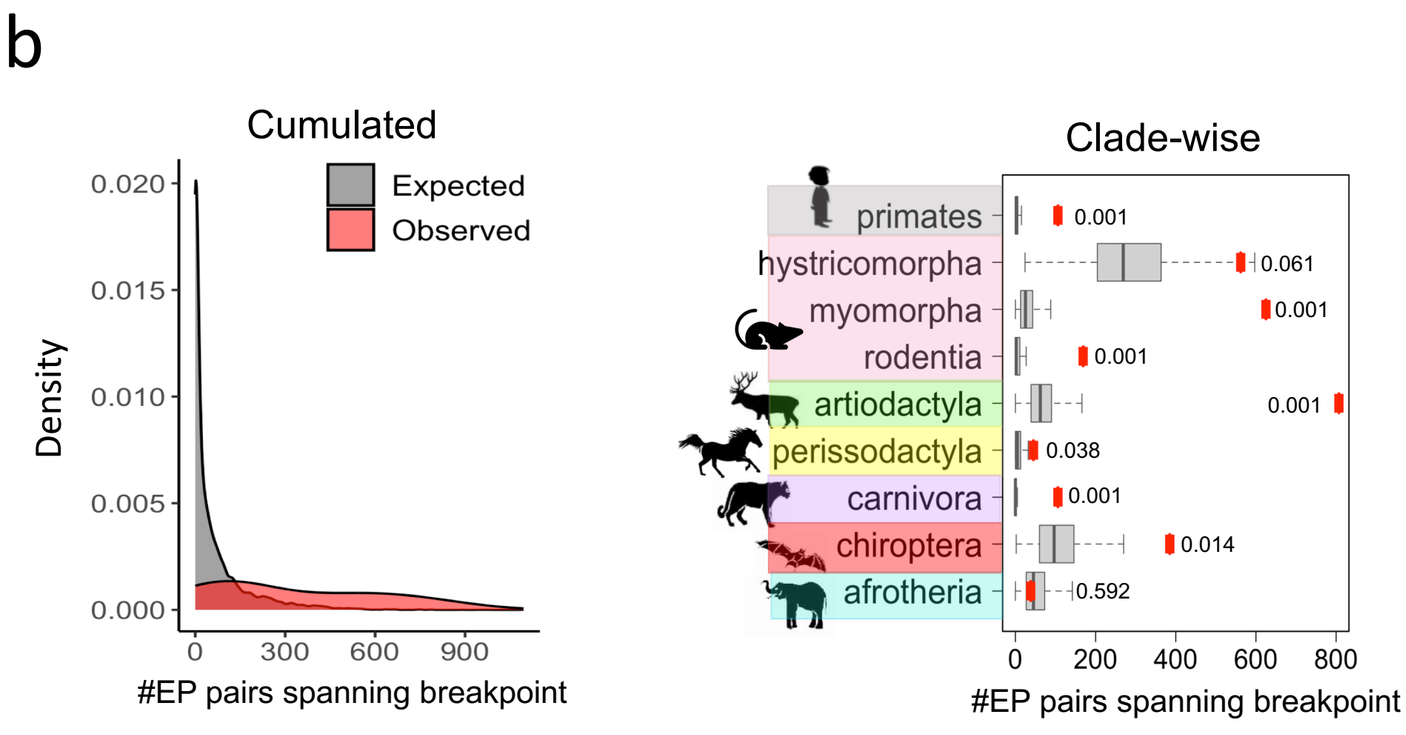
b
Cumulated
Expected
Observed
Density
#EP pairs spanning breakpoint
Clade-wise
primates
hystricomorpha
myomorpha
rodentia
artiodactyla
perissodactyla
carnivora
chiroptera
afrotheria
0.001
0.061
0.001
0.001
0.001
0.038
0.001
0.014
0.592
#EP pairs spanning breakpoint

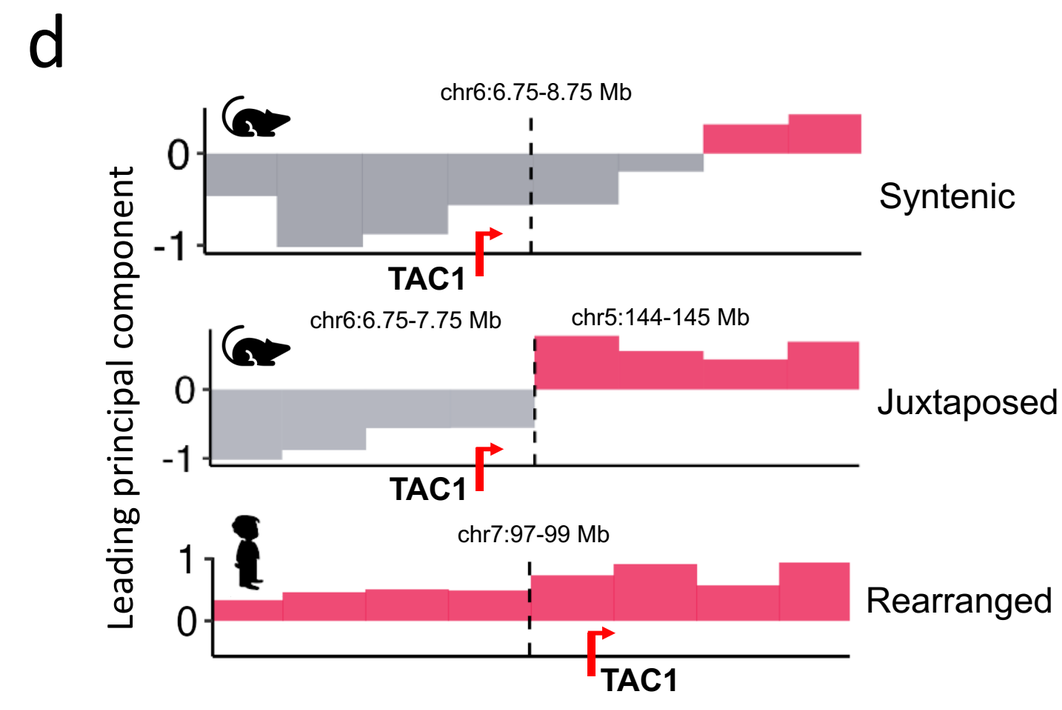
d
chr6:6.75-8.75 Mb
Syntenic
TAC1
chr6:6.75-7.75 Mb
chr5:144-145 Mb
Juxtaposed
TAC1
chr7:97-99 Mb
Rearranged
TAC1
Leading principal component

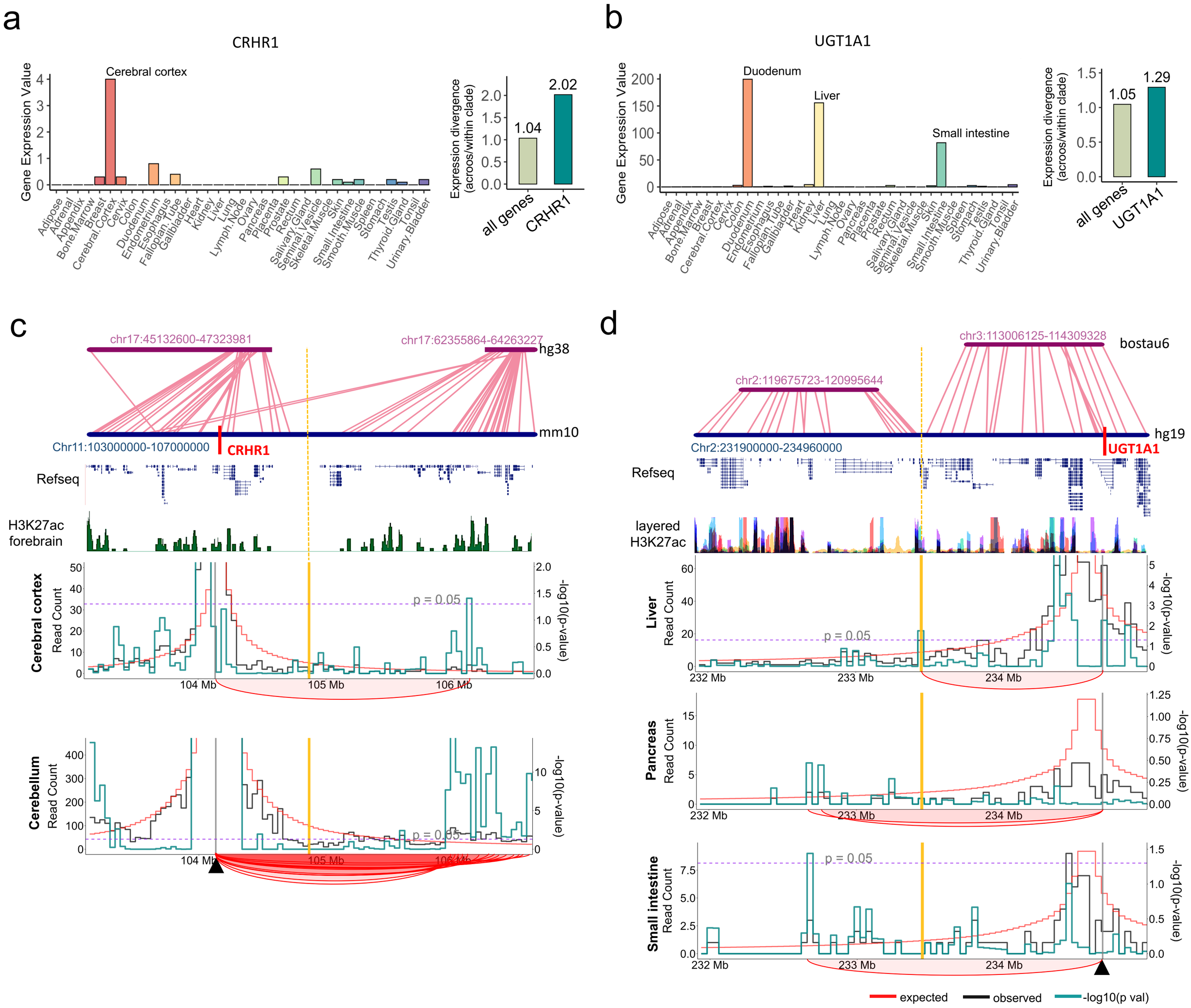
a
CRHR1
Cerebral cortex
Gene Expression Value
Expression divergence (acroos/within clade)
1.04
2.02
all genes
CRHR1
b
UGT1A1
Duodenum
Liver
Small intestine
Gene Expression Value
Expression divergence (acroos/within clade)
1.05
1.29
all genes
UGT1A1
c
chr17:45132600-47323981
chr17:62355864-64263227
hg38
mm10
Chr11:103000000-107000000
CRHR1
Refseq
H3K27ac forebrain
Cerebral cortex
Cerebellum
Read Count
-log10(p-value)
p = 0.05
104 Mb
105 Mb
106 Mb
d
chr3:113006125-114309328
bostau6
chr2:119675723-120995644
hg19
Chr2:231900000-234960000
UGT1A1
Refseq
layered H3K27ac
Liver
Pancreas
Small intestine
Read Count
-log10(p-value)
p = 0.05
232 Mb
233 Mb
234 Mb
expected
observed
-log10(p val)

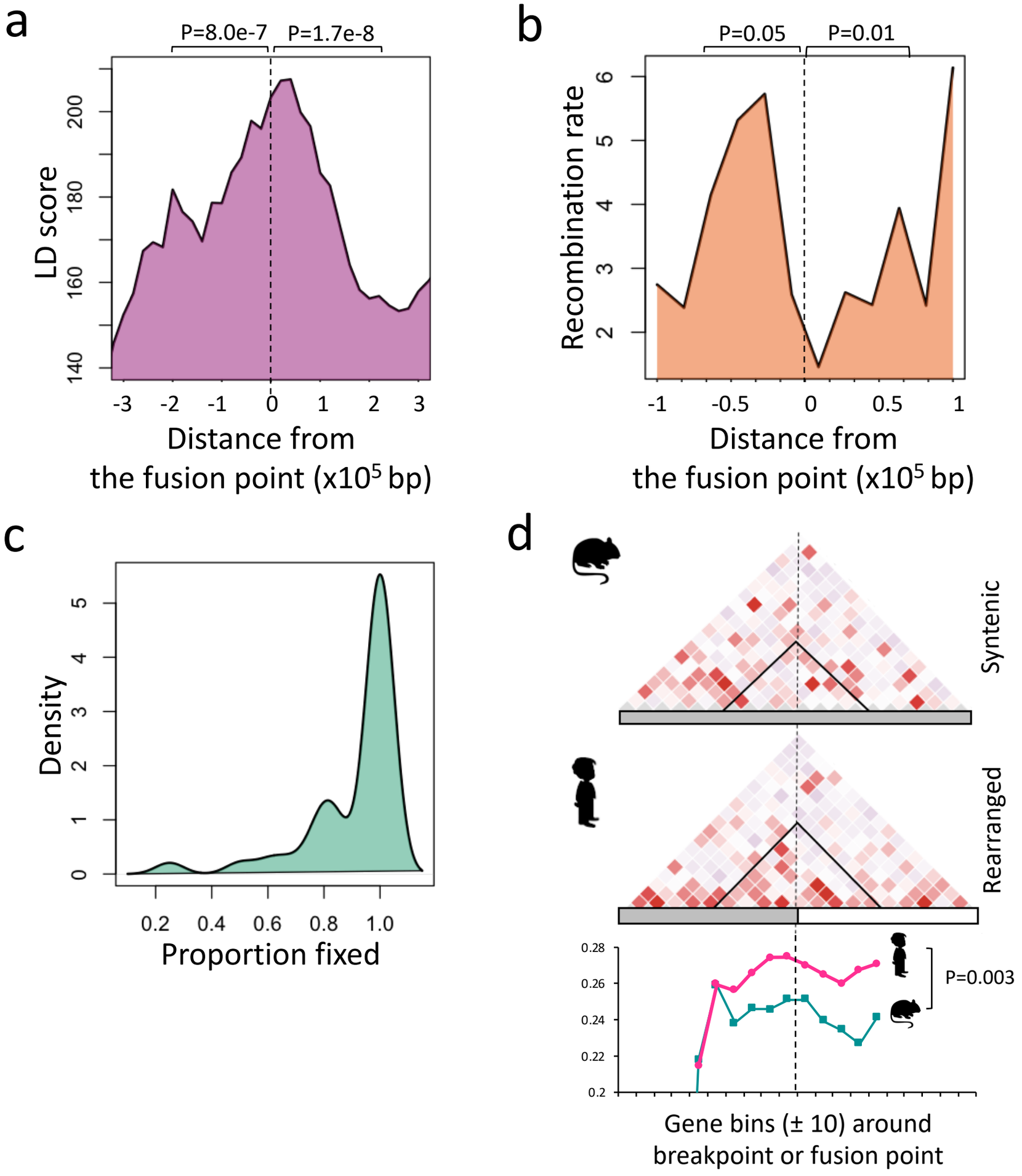
a
P=8.0e-7
P=1.7e-8
LD score
140
160
180
200
-3
-2
-1
0
1
2
3
Distance from
the fusion point (x10^5 bp)
b
P=0.05
P=0.01
Recombination rate
2
3
4
5
6
-1
-0.5
0
0.5
1
Distance from
the fusion point (x10^5 bp)
c
Density
0
1
2
3
4
5
0.2
0.4
0.6
0.8
1.0
Proportion fixed
d
Syntenic
Rearranged
0.28
0.26
0.24
0.22
0.2
P=0.003
Gene bins (± 10) around
breakpoint or fusion point

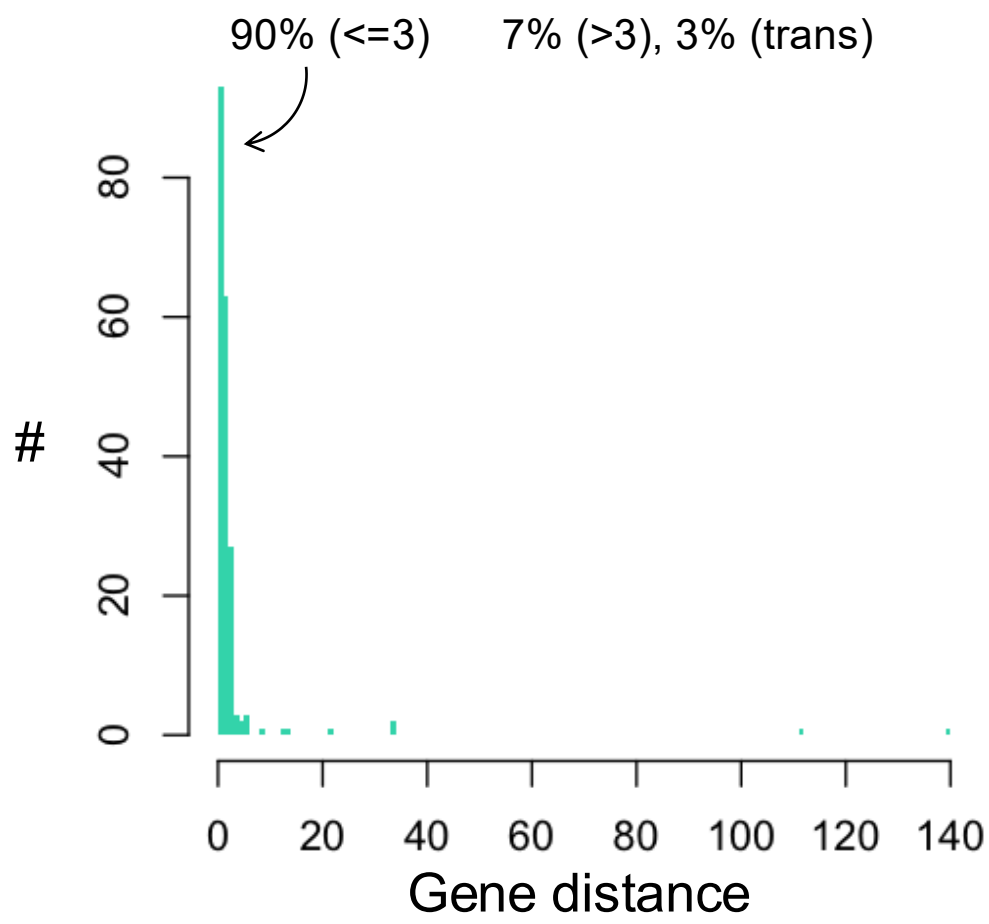

Figure S1. Distribution of gene-distances (#genes) between genes flanking the clade-specific breakpoints in the common ancestor of placental mammals

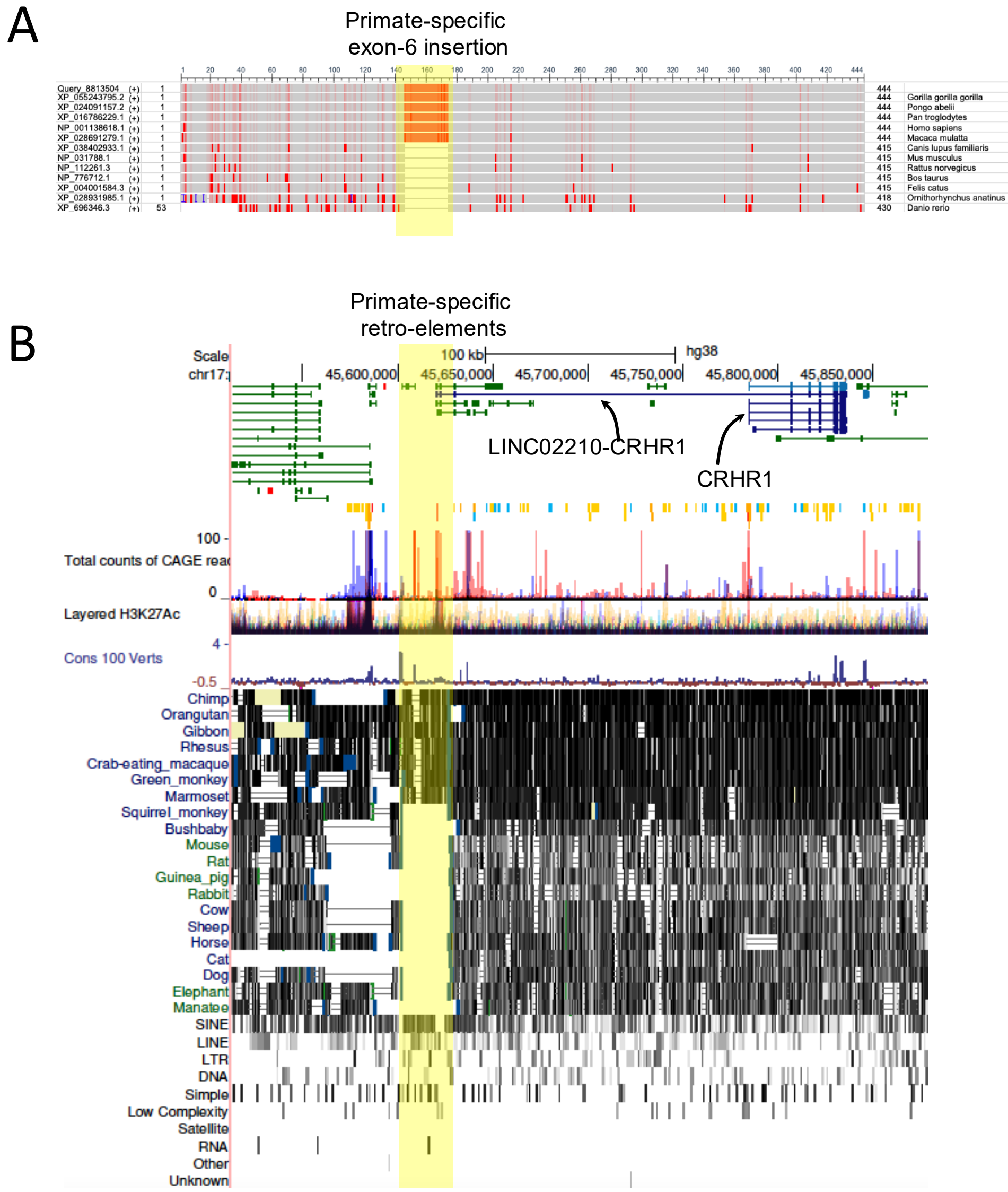

Figure S2. (A) Primate specific insertion of exon-6 in the CRHR1 protein. (B) Primate-specific insertion of re tro-viral elements upstream to the CRHR1 gene and at the promoter of a LINC RNA.

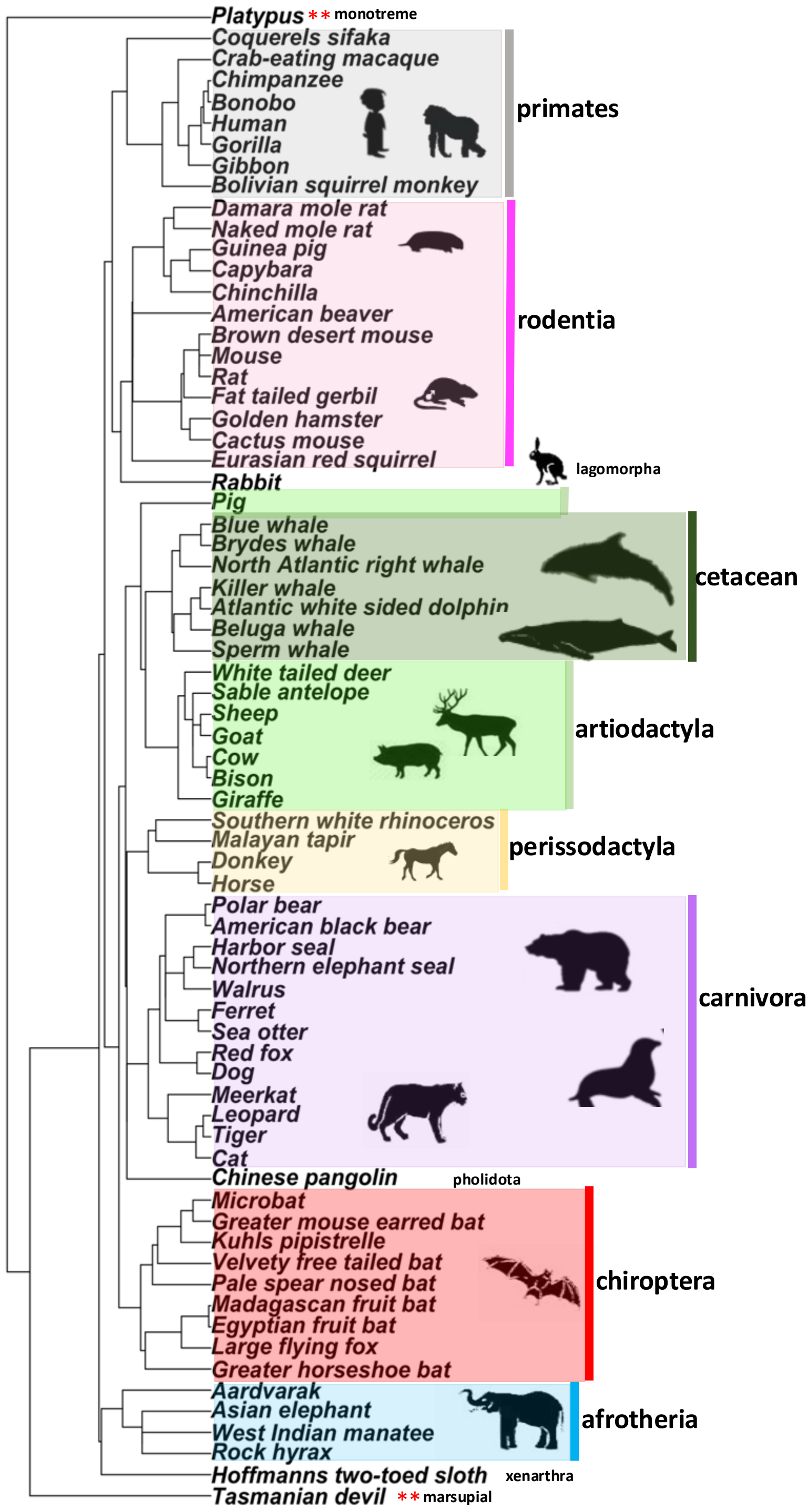

Figure S3. Phylogenetic tree of species analyzed in the study

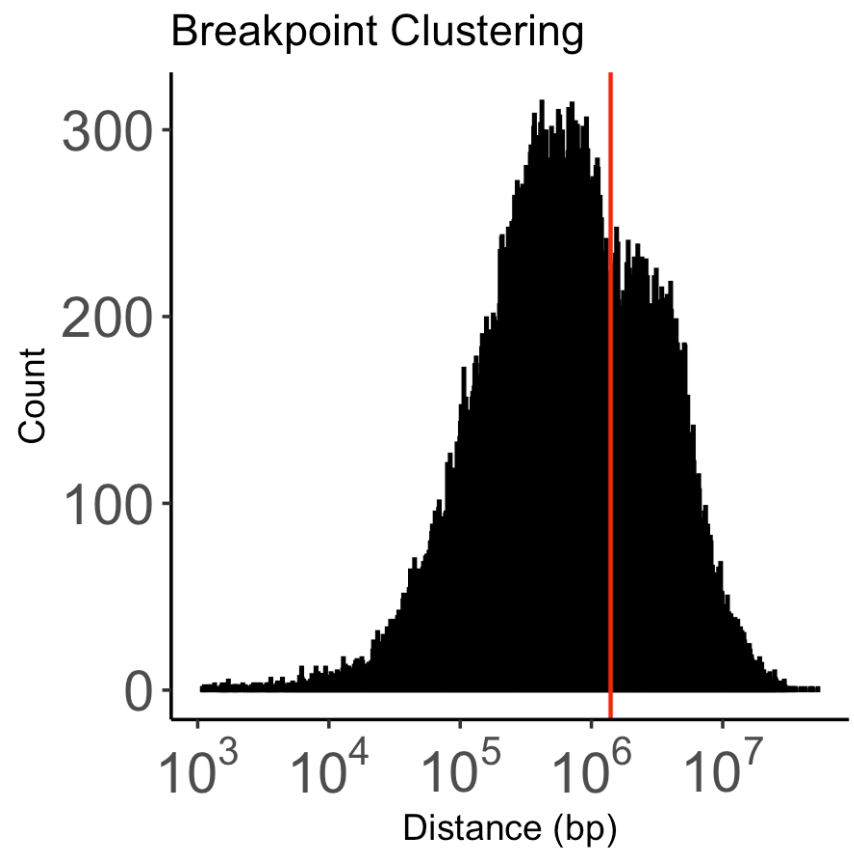

Figure S4. Distribution of inter-breakpoint distances across species. Vertical bar marks the cut-off of 1.4Mb